Microglial NLRP3 inflammasome activation upon TLR2 and TLR5 ligation by distinct α-synuclein assemblies

Hannah Scheiblich, Luc Bousset, Stephanie Schwartz, Angelika Griep, Eicke Latz, Ronald Melki, Michael T Heneka

To: The Journal of Immunology

Microglial NLRP3 inflammasome activation upon TLR2 and TLR5 ligation by distinct α-synuclein assemblies

Running title: NLRP3 inflammasome activation by α-syn in microglia

Hannah Scheiblich [*, †], Luc Bousset [‡], Stephanie Schwartz [*], Angelika Griep [†], Eicke Latz [§], Ronald Melki [‡], Michael T. Heneka [*, †]

[*] Department of Neurodegenerative Disease and Gerontopsychiatry/Neurology, University of Bonn - Medical Center, Bonn, Germany

[†] German Center for Neurodegenerative Diseases (DZNE), Bonn, Germany

[‡] Institut François Jacob, MIRCen, CEA and Laboratory of Neurodegenerative Diseases, CNRS, Fontenay-aux-Roses, France

[§] Institute of Innate Immunity, University of Bonn - Medical Center, Bonn, Germany

Correspondence: Prof. Dr. Michael T. Heneka
Mail: michael.heneka@ukbonn.de
Phone: +49 228 28713091
Fax: +49 228 28713166

Email:
H.S.: hannah.scheiblich@ukbonn.de
L.B.: luc.bousset@cnrs.fr
S.S.: stephanie.schwartz@ukbonn.de
A.G.: angelika.griep@dzne.de
E.L.: eicke.latz@uni-bonn.de
R.M.: ronald.melki@cnrs.fr
M.T.H.: michael.heneka@ukbonn.de

Abstract

Parkinson's disease (PD) is the second most common age-related neurodegenerative disorder characterized by the formation of cellular inclusions inside neurons that are rich in an abnormal form of the protein α-synuclein (α-syn). Microglia are the CNS resident immune cells that react to misfolded proteins through pattern recognition receptor ligation and activation of signaling transduction pathways. Here, we studied activation of primary microglia isolated from wild-type mouse by distinct α-syn forms and their clearance. Internalization of α-syn monomers and oligomers efficiently activated the NLRP3 inflammasome via Toll-like receptor-2 and -5 ligation, thereby acting on different signaling checkpoints. We found that primary microglia effectively engulf α-syn, but hesitate in its degradation. NLRP3 inhibition by the selective inhibitor CRID3 and NLRP3 deficiency improved the overall clearance of α-syn oligomers. Together, these data show that distinct α-syn forms exert different microglial NLRP3 inflammasome activation properties, thereby compromising its degradation which can be prevented by NLRP3 inhibition.

Keywords

microglia, α-synuclein, NLRP3 inflammasome, Toll-like receptors, clearance

Key points

- α-syn monomers and oligomers efficiently activated the NLRP3 inflammasome via TLR2
- activation of the NLRP3 inflammasome compromised the α-syn clearance capacity
- NLRP3 inhibition improved the overall clearance of α-syn oligomers

Introduction

Parkinson's disease (PD) is the most common movement disorder and, after Alzheimer's disease, the second most common neurodegenerative disease. PD is mainly characterized by the presence of intraneuronal cytoplasmic inclusions called Lewy bodies (LB) rich in aggregated α-synuclein (α-syn) (1, 2). α-syn is a 14 kDa protein with no defined structure (3). The monomeric form of the protein progressively forms oligomeric structures and insoluble fibrillary complexes that, together with crowded organellar components (1), accumulate in LBs under pathological conditions. The fibrillar forms of α-syn interfere with neuronal functioning by affecting the normal distribution of important membrane proteins (4), disrupting neurotransmitter release (5), impairing mitochondrial function (6–8), blocking intracellular vesicle transport (9, 10), affecting endo-lysosomal compartment integrity (11), and compromising protein-degradation mechanisms (12), thereby inducing toxicity, eventually leading to neuronal injury and degeneration. Even though α-syn aggregates are first found in neurons evidence suggests that neuronal cell death and spreading of pathology will expose these proteins to the environment, thereby activating surrounding immune cells.

Being the brain's primary innate immune cells, microglia contribute to cerebral homeostasis by sensing changes in their immediate environment, clearing cellular debris and providing neurotrophins (13). Upon ligation of pattern recognition receptors (PRRs), microglia become activated and execute an inflammatory response which, in case it persists, causes chronic neuroinflammation and neuronal damage (13, 14). Evidence for such a chronic neuroinflammatory response can be found in brains of PD patients and other synucleinopathies, where microglia activation occurs in all brain regions where aggregated α-syn accumulates (15–17). In keeping with this, α-syn has been shown to induce excessive microglial activation and inflammatory activity.

Interleukin-1β (IL-1β) is the most extensively studied pro-inflammatory cytokine, which has been linked to various disorders of the CNS (18, 19) . In PD, α-syn has been shown to induce the microglia-derived IL-1β secretion following NLRP3 inflammasome activation (20–22). Likewise, NLRP3 inflammasome inhibition prevented α-syn pathology and dopaminergic neurodegeneration in PD-related mouse models (23). *In vitro*, IL-1β is synthesized by microglia as a precursor (pro-IL-1β) in response to pathogen-associated molecular patterns (PAMPs) such as lipopolysaccharide (LPS) that is acting via Toll-like receptor (TLR) ligation (24, 25). This step, which is referred as "priming" is required to induce the expression of the inflammasome components: the pattern recognition receptor NOD-like receptor pyrin domain containing 3 (NLRP3), apoptosis-associated speck-like protein (ASC), and the pro-caspase-1. A second stimulus which is referred to as "activation" results in the formation and activation of cytosolic multiprotein complexes called inflammasomes (19, 26, 27) that process the precursor

pro-IL-1β to its mature IL-1β form that is rapidly secreted from the cell into its microenvironment (28).

To unravel microglial activation by different α-syn forms, we used structurally and functionally well characterized human α-syn monomers, oligomers and two different fibrillar polymorphs that have been shown to trigger distinct synucleinopathies (29, 30) and tested their potential to activate microglia through PRR ligation. We further analyzed how microglia survival is affected upon exposure to monomeric, oligomeric and fibrillar α-syn and how microglia deal with the clearance of α-syn assemblies. Here, we present evidence that α-syn monomers and oligomers are able to prime and activate the NLRP3 inflammasome through TLR2 and TLR5 ligation, leading to NLRP3 inflammasome-dependent IL-1β secretion thereby inhibiting α-syn clearance. In addition, the microglial survival was not affected by the different α-syn forms, thus, largely excluding pyroptotic cell death within the tested time period.

Material and Methods

Animals

Wild-type (WT, Charles River Laboratories, Inc., Wilmington, MA, USA) and NLRP3-deficient (Millenium Pharmaceuticals, Cambridge, MA, USA) animals were all of the C57BL/g genetic background. Mice were housed under standard conditions at 22 °C and a 12 hrs light-dark cycle with free access to food and water. Animal care and handling was performed according to the guidelines of animal welfare as laid down by the German Research Council (DFG) and approved by the local ethical committees.

Cell culture

Primary microglia cells were isolated by the method of Giulian and Baker (31). Briefly, brains from neonatal mice were stripped of the meninges and dissociated using mechanical shearing and trypsin (Life Technologies, Carlsbad, CA, USA). Cells of two brains were plated on poly-L-lysine (PLL, Sigma-Aldrich by Merck KGaA, Darmstadt, Germany) coated T75 culture flasks (Greiner bio-one, Kremsmünster, Austria) and cultivated in DMEM (Gibco by Thermo Fisher Scientific, Waltham, MA, USA) supplemented with 10% heat-inactivated fetal calf serum (FCS; Gibco) and 1% penicillin/streptomycin (P/S; Gibco). On the next day cells were washed three times with DPBS (Gibco) to remove cellular debris and cultured with DMEM supplemented with 10% FCS, 1% P/S and 1% L929 conditioned medium as a source of growth factors. After 7-10 days loosely attached mature microglia were shaken off the astrocytic layer with a repetition of the harvesting procedure all two to three days for up to three times. For experiments, primary microglia were seeded into well plates and allowed to adhere overnight in DMEM supplemented with 10% FCS and 1% P/S. On the next day medium was changed to serum-free DMEM complemented with 1% N-2 supplement (Gibco) and microglia were allowed to rest for another 24 hrs before experiments were performed.

α-synuclein assemblies generation

Human wild-type α-syn was expressed in E. coli BL21 DE3 CodonPlus cells (Stratagene, San Diego, CA, USA) and purified as described previously (32). To assemble human wild-type α-syn into the fibrillar polymorph “Fibrils”, the protein (100 µM) was incubated in 50 mM Tris–HCl, pH 7.5, 150 mM KCl at 37°C under continuous shaking in an Eppendorf Thermomixer set at 600 rpm for 5 days (29). The assembly reaction was followed by withdrawing aliquots (20 µl) from the assembly reaction at different time intervals, mixing them with Thioflavin T (10 µM final) and recording the fluorescence increase on a Cary Eclipse Fluorescence Spectrophotometer (Varian Medical Systems Inc., Palo Alto, CA, USA) using an excitation wavelength = 440 nm, an emission wavelength = 480 nm and excitation and emission slits set

at 5 and 10 nm, respectively. To label α-syn fibrils with extrinsic fluorophores, the fibrils were centrifuged twice at 15,000 *g* for 10 min and re-suspended twice in PBS at 1,446 g/L and two molar equivalents of ATTO-488 NHS-ester (Atto-Tec GmbH, Siegen, Germany, #AD 488-35) fluorophore in DMSO were added. The mix was incubated for 1h at room temperature. The labeling reactions were arrested by addition of 1mM Tris pH 7.5. The unreacted fluorophore was removed by a final cycle of two centrifugations at 15,000 *g* for 10 min and resuspensions of the pellets in PBS. The fibrillar nature of α-syn was assessed by Transmission Electron Microscopy (TEM) after adsorption of the fibrils onto carbon-coated 200 mesh grids and negative staining with 1% uranyl acetate using a Jeol 1400 transmission electron microscope. The images were recorded with a Gatan Orius CCD camera (Gatan, Pleasanton, CA, USA). The resulting α-syn fibrils were fragmented by sonication for 20 min in 2-ml Eppendorf tubes in a Vial Tweeter powered by an ultrasonic processor UIS250v (250 W, 2.4 kHz; Hielscher Ultrasonic, Teltow, Germany) to generate fibrillar particles with an average size 42-52 nm as assessed by TEM analysis.

Measurement of cytokine secretion

Cytokine release was determined using the mouse IL-1 beta/IL-1F2 DuoSet ELISA (DY401, R&D Systems, Minneapolis, MN, USA), mouse TNF-alpha DuoSet ELISA (DY410, R&D Systems), mouse IL-6 DuoSet ELISA (DY406, R&D Systems), mouse IL-10 DuoSet ELISA (DY417, R&D Systems), and mouse CXCL2/MIP-2 DuoSet ELISA (DY452, R&D Systems). Primary microglia (7.5 x 10^4 cells/well) were seed into 96-well plates and allowed to adhere overnight. Microglia were used unprimed or primed for 3 hrs prior to experiments with 10 ng/ml (≙100 EU/ml) lipopolysaccharide (LPS; InvivoGen, San Diego, CA, USA) before cells were washed with DPBS and treated with α-syn monomers and different assemblies and BSA as a protein control. For TLR neutralizing experiments, microglia were treated 5 µg/ml mouse anti-TLR2 (InvitroGen), mouse anti-TLR4 (Invitrogen), or rat anti-TLR5 (InvivoGen) in conjunction with 2 µM α-syn assemblies. Supernatants were assayed after 24 hrs treatment according to the manufacturer's protocol. Optical density was determined at 450 nm photometrically with a microplate reader (Infinite M200, Tecan, Männedorf, Switzerland). Concentrations of the secretion of the different cytokines were calculated by interpolation using a respective cytokine specific standard curve.

The expression profile of different cytokines and chemokines in response to different α-syn species was analysed using a Proteome Profiler™ Array (ARY020, R&D Systems). Primary microglia (2 x10^6 cells/well) were seed into 6-well plates and allowed to adhere overnight. Microglia were used unprimed or primed for 3 hrs prior to experiments with 10 ng/ml (≙100 EU/ml) LPS before cells were washed with DPBS and treated with α-syn monomers and different assemblies for 24 hrs. The Proteome Profiler™ Array was performed according to the

manufacturer's protocol using 1 ml of cell supernatant per condition. After overnight incubation with the sample/antibody mixture, membranes were washed three times with the wash buffer and incubated with the fluorescent near-infrared secondary antibody IRDye® 680LT Streptavidin (1:10,000 in 3% BSA, LI-COR Biosciences, Lincoln, NE, USA) for 30 min at RT. Capture spots were then visualized with the Odyssey CLx Imaging System (LI-COR Biosciences) and quantified using Image Studio (LI-COR Biosciences).

Precipitation of supernatant samples

For detection of the cleaved caspase-1 subunit p20 in the supernatant of treated primary microglia cultures we performed a protein precipitation to concentrate the sample as described by Jakobs and colleagues (33). Briefly, primary microglia (1.5 x 10^6 in 2 ml medium) were cultured for 24 hrs in 6-well plates under control conditions or in medium containing chemical compounds. After harvesting the supernatants 500 µl methanol and 125 µl chloroform were added to 500 µl supernatant and vortexed vigorously. After 5 min centrifugation at 13,000 g the upper aqueous phase was removed and replaced by 500 µl methanol. Samples were vortexed again and centrifuged for 5 min at 13,000 g. Subsequently, supernatants were removed and pellets were dried for 5 min in a vacuum dryer. The pellet was than resuspended in 20 µl 2x loading buffer and denaturated for 3 min at 95 °C. Samples were then subjected to Western blot analysis.

Western blot

For lysate collection, primary microglia (2 x 10^6) were cultured in 6-well plates under control conditions or in medium containing different α-syn assemblies for 24 hrs before supernatants (for protein precipitation) were collected and cells were washed and scraped off the well with ice cold PBS containing 1x protease and phosphatase inhibitor cocktails (Thermo Fisher Scientific). After pelleting the cells for 5 min at 10,000 g PBS was completely removed and cells were lysed in ice cold RIPA buffer (50 mM Tris-HCl, 1% Triton X-100, 0.5% Na deoxycholate, 0.1% sodium dodecyl sulfate (SDS), 150 mM NaCl, pH 8.0) containing 1x protease inhibitor cocktails for 15 min on ice. Lysates were centrifuged 5 min at 4 °C and 10,000 g and supernatants were frozen and kept in -20 °C until use.

Cell lysates and samples from protein precipitation were separated by a NuPAGE® 4-12% Bis-Tris Gel (Invitrogen by Thermo Fisher Scientific) and transferred to a nitrocellulose blotting membrane (0.2 µm; GE Healthcare Life Sciences, Freiburg, Germany). Membranes were washed with Tris-buffered saline supplemented with Tween-20 (TBST, 10 mM Tris-HCl, 150 mM NaCl, 0.05% Tween-20, pH 8.0). Membrane surface was blocked with 3% BSA in TBST for 30 min at RT. Membranes were then incubated with the rat anti-caspase-1 antibody (1:1,000; clone 4B4, Genentech, CA, USA), rabbit anti-Asc (AL177, 1:1,000, AdipoGen, San

Diego, USA), mouse anti-NLRP3 (1:500, AdipoGen), rabbit anti-MyD88 (1:500, Cell Signaling Technologies), rabbit anti-NF-κB p65 (1:500, Cell Signaling Technologies), or mouse anti-α-tubulin (1:2,000; Thermo Fisher Scientific) overnight at 4 °C. After three washing steps á 5 min with TBST the fluorescent near-infrared secondary antibodies IRDye® 800CW Goat anti-Rat IgG (H + L) (1:10,000 in 3% BSA, LI-COR Biosciences, Lincoln, NE, USA) and IRDye® 680LT Donkey anti-Mouse IgG (H + L) (1:10,000 in 3% BSA, LI-COR Biosciences) were applied for 30 min at RT. Proteins were then visualized with the Odyssey CLx Imaging System (LI-COR Biosciences) and quantified using Image Studio (LI-COR Biosciences).

Immunocytochemistry

Cultures were fixed in 4% paraformaldehyde (PFA, Sigma-Aldrich) dissolved in PBS (Biochrom GmbH, Berlin, Germany) for 15 min and permeabilized by washing them tree times for 5 min with PBS containing 0.1% Triton X-100 (PTX). Blocking solution containing PTX and 5% normal goat serum (Vector Laboratories, Burlingame, CA, USA) was applied for 30 min. The primary antibodies rabbit anti-ASC (1:250; #D2W8U, Cell Signaling Technologies, Danvers, MA, USA) and rat anti-CD11b (1:250; Serotec by Bio-Rad) were applied for 1 h followed by three washing steps. The secondary antibodies goat anti-rabbit-AlexaFluor594 (1:250; Invitrogen) and goat anti-rat-AlexaFluor594 (1:250; Invitrogen) were applied for 30 min. The LysoTracker™ Red DND-99 (Thermo Fisher Scientific) was applied according to the manufacturer's protocol. 4',6-Diamidino-2'-phenylindol-dihydrochloride (DAPI, Sigma-Aldrich) was used for nuclear counterstaining at 0.1 mg/mL for 20 min in PBS. Images were taken using a 60x oil-objective.

Phagocytosis assay

To assess microglial phagocytosis, primary microglia (3.5 x 10^5 cells/well) were seeded to 24-well plates and allowed to adhere. Microglia were treated with 1 µM Atto488-labeled α-syn assemblies and incubated for 5-15 min. Phagocytosis was stopped by one washing steps with PBS to remove free α-syn and cells were harvested using 0.5% trypsin (Gibco). Blocking solution containing PBS and FCS (1:1 ratio) was applied for 10 min on ice. Cells were then labelled with the APC anti-mouse/human CD11b antibody (1:100; #101212, BioLegend, San Diego, CA, USA) for 30 min in FACS solution (PBS supplemented with 2% FCS) on ice. Following labelling, cells were collected, resuspended in 300 µl ice cold FACS solution, and measured by flow cytometry using the FACS CANTO II and the FACSDIVA™ software (Becton Dickinson, Heidelberg, Germany). Phagocytosis was then analysed and quantified using FlowJo, LLC (v3.05470, Ashland, OR, USA).

Microscopy and data analysis

All experiments were examined with a Nikon Eclipse Ti fluorescence microscope (Nikon, Tokyo, Japan). Acquired images were processed using NIS-elements 4 (Nikon) and Fiji ImageJ (Wayne Rusband, National Institute of Health, USA). Data were evaluated using Graph Pad Prism and presented as mean ± SEM of at least three independent experiments with two to three replicates. An outlier test was performed and data were analysed for Gaussian distribution. When data passed the normality test statistical comparisons of controls versus treatments were performed with one-way ANOVA or two-way ANOVA followed by a Tukey's test. Otherwise, data were analysed with the Kruskal-Wallis test and a Dunn's post hoc test for non-parametric data. Levels of significance are indicated as *$p < 0.05$; **$p < 0.01$; ***$p < 0.001$; ****$p < 0.0001$.

Results

We and others recently demonstrated that monomeric α-syn populates oligomeric species (34–36) and assembles into structurally distinct fibrillar polymorphs that trigger when injected to rodents the hallmarks of two distinct synucleinopathies, PD or MSA (29, 30). These assemblies expose different polypeptide chains at their surfaces and as a consequence exhibit differential tropism to neurons (37). How different α-syn assemblies, that form in the brain of patients target and activate glial cells is still unclear. To investigate whether structurally different α-syn polymorphs induce the NLRP3 inflammasome in microglia, we exposed primary mouse microglia to well-characterized recombinant human α-syn assemblies (29, 30). To investigate the potential impact on microglial activation of different forms of α-syn (Fig. 1 A-K), we performed all experiments on microglia with and without pre-exposure to the inflammogen LPS (10 ng/ml (≙100 EU/ml), 3 hrs) (Fig. S1 A). All α-syn species were initially validated as endotoxin-free (Fig. S1 B) and dose response curve analysis were performed (Fig. S1 C). The following stimulation experiments were performed using 2 μM α-syn which has been the lowest concentration inducing NLRP3 inflammasome activation in unprimed conditions (Fig. S1 C), and has been confirmed as being non-cytotoxic using the XTT viability assay in conjunction with an LDH assay (Fig. S1 D-E). BSA was tested in parallel to α-syn as a protein control.

α-synuclein activates the NLRP3 inflammasome via TLR2 and TLR5 ligation and induces the release of IL-1β

IL-1β release is mediated by activation of the NLRP3 inflammasome upon assembly of NLRP3, ASC, and pro-caspase-1. We assessed conditioned medium of primary microglia exposed to monomeric, oligomeric or fibrillar polymorphs further referred as “fibrils” and “ribbons” for IL-1β concentrations at 6 and 24 hrs. Even though there was no detectable IL-1β release at 6 hrs (Fig. 1 L), exposure to α-syn monomers and oligomers was sufficient to induce pro-IL-1β (Fig. S2 A) and mature IL-1β (Fig. 1 M) in unprimed microglia at 24 hrs. NLRP3 inflammasome activation was confirmed by immunoblot detection showing increased levels of cleaved caspase-1 compared to their controls (Fig. 1 N-P). Interestingly, α-syn monomers and oligomers upregulated the expression of NLRP3 (Fig. 1 Q), while the expression of the adapter protein ASC showed only a slight increase upon treatment with ribbons (Fig. 1 R). Using immunoblot analysis we found the expression of the universal adapter protein MyD88 upregulated upon treatment with monomeric and oligomeric α-syn (Fig. 2 A), which further activates the transcription factor NF-κB. Even though there was no detectable difference in the NF-κB expression levels (Fig. 2 B), immunostainings revealed the translocation of NF-κB p65 into the nucleus in microglia exposed to α-syn monomers (Fig. 2 C, arrows, Fig. 2 D).

To elucidate by which PRR ligation α-syn monomers and oligomers activate the NLRP3 inflammasome, three TLR neutralizing antibodies including anti-mouse TLR2, anti-mouse TLR4, and anti-rat TLR5 were tested (Fig. 2). Unprimed microglia were exposed to different forms of α-syn in the presence or absence of the respective TLR neutralizing antibodies (Fig. 2 E-H). Isotype specific antibodies were used as negative control. For a better clarity we calculated the percent of neutralization to the α-syn treated control levels (Ø). We found that anti-TLR2 and anti-TLR5 attenuated the IL-1β release by about 50% to α-syn treated control levels and isotype specific controls, in microglia exposed to α-syn monomers (Fig. 2 E) and oligomers (Fig. 2 F). α-syn fibrils (Fig. 2 G) and ribbons (Fig. 2 H) did not increase IL-1β levels. We confirmed the inhibitory effects of TLR neutralization on NLRP3 inflammasome activation by immunoblot analysis. Both, TLR2 and TLR5 neutralization inhibited the α-syn monomer- and oligomer-induced cleavage of caspase-1 (Fig. 2 I-J), while only TLR2 neutralization blocked the induction of NLRP3 (Fig. 2 I, K). Caspase-1 p45 and ASC expression remained unchanged (Fig. S2 B-C). Importantly, the ability of α-syn to prime and activate the NLRP3 inflammasome was completely abolished in primary microglia derived from TLR2 knockout animals (Fig. S2 D-E) as confirmed by immunoblot analysis and ELISA readings. Importantly, caspase-1 cleavage inhibition by the NLRP3 inflammasome inhibitor CRID3 largely suppressed NLRP3 inflammasome activation and IL-1β secretion by α-syn treated unprimed microglia (Fig. S3).

Since NLRP3 inflammasome mediated IL-1β production usually requires a priming step, we investigated if a classical priming condition would influence the degree and pattern of α-syn-induced NLRP3 activity. Therefore, we pre-stimulated primary microglia for 3 hrs with 10 ng/ml LPS before treating the cells with α-syn. LPS priming did not change the IL-1β release within 6 hrs of treatment (Fig. 3 A), but largely increased the secretion of IL-1β at 24 hrs when microglia were exposed to α-syn monomers, oligomers or fibrils (Fig. 3 B). We performed immunoblot analysis to check for the activation of the NLRP3 inflammasome (Fig 3 C). Even though caspase-1 p45, NLRP3, and ASC expression levels remained unchanged after exposure to α-syn monomers and assemblies for 24 hrs (Fig. 3 C-G), we found significantly increased secretion levels of the active caspase-1 subunit p20 in response to monomers and oligomers (Fig. 3 E). Most importantly, NLRP3 knockout and caspase-1 cleavage inhibition by CRID3 largely suppressed NLRP3 inflammasome activation and IL-1β secretion by α-syn treated LPS-primed microglia (Fig. S4). In addition to caspase-1 cleavage, inflammasome activation is characterized by formation of ASC specks (38) that can be visualized by intra- and extracellular ASC-immunopositive specks (Fig. 3 H). LPS-primed microglia displayed an increase of ASC specks at 24 hrs after exposure to α-syn monomers (Fig. 3 I) with a partial co-localization of α-syn monomers and ASC specks (Fig. 3 J). Again, we used TLR

neutralization antibodies to check for PRR ligation of α-syn monomers and distinct assemblies under primed conditions. For a better clarity we calculated the percent of neutralization to the α-syn treated control levels (Ø). Using anti-TLR neutralization antibodies on LPS-primed α-syn treated microglia we confirmed that the IL-1β release of microglia treated with α-syn monomers (Fig. 3 K), oligomers (Fig. 3 L) and fibrils (Fig. 3 M) was attenuated upon neutralization of TLR2, whereas ribbons neither increased IL-1β nor did TLR neutralization showed any effect (Fig. 3 N). TLR4 and TLR5 neutralization did not change the α-syn-induced IL-1β release of LPS-primed microglia (data not shown).

In addition to IL-1β, we checked for the release of other pro- and anti-inflammatory cytokines (Fig. S5). Initially, we exposed supernatants of primary microglia with or without prior LPS-priming to a proteome profile array to get an overview about the inflammatory profile of the cells (Fig. S5 A). We found that α-syn monomer, oligomers and fibrils augmented the release of various pro-inflammatory cytokines (Fig. S5 A, left panel) which was further amplified by prior LPS-priming (Fig. S5 A, right panel). Ribbons showed no effect on the cytokine secretion. To confirm these findings and to quantify the cytokine release in more detail we selected certain cytokines and performed ELISA readings on supernatants of primed and unprimed microglia exposed to α-syn monomers and distinct assemblies.

Interestingly, we found that α-syn monomers, oligomer and fibrils induced the release of TNFα (Fig. S5 B), IL-6 (Fig. S5 C), IL-10 (Fig. S5 D), NO (Fig. S5 E), and CXCL2 (Fig. S5 F) whereby the release was further amplified by prior LPS priming. Again, ribbons had no effect on the cytokine secretion. In order to confirm the involvement of TLRs in α-syn-induced immune signalling, we performed TLR neutralizing experiments on unprimed microglia and used CXCL2 secretion as another read-out (Fig. S5 G-J). For better clarity we calculated the percent of neutralization to the α-syn treated control levels (Ø). Again, we found that neutralization of TLR2 and TLR5 attenuated the release of CXCL2 from microglia exposed to α-syn monomers (Fig. S5 G) and oligomers (Fig. S5 H). In line with that, TLR2 and TLR5 neutralization decreased the CXCL2 release in response to fibrils (Fig. S5 I) and ribbons (Fig. S5 J). We did not find any indication for an involvement of TLR4 in α-syn-induced CXCL2 release.

Together, our data show a TLR2- and TLR5-mediated inflammatory signalling in microglia dependent on α-syn structural characteristics. Moreover, to our knowledge, this is the first evidence for an involvement of TLR5 in monomeric and oligomeric α-syn-induced microglial activation. In addition to IL-1β, we found various other inflammatory agents upregulated by α-syn including TNFα, IL-6, IL-10, NO, and CXCL2 further underlining differential pro-inflammatory properties of distinct α-syn species (Fig. S5).

NLRP3 modulates the uptake and degradation of α-syn in microglia

To characterize and compare the microglial uptake of different α-syn forms, cells were exposed for 5, 10 or 15 min to fluorescently labelled α-syn monomers, oligomers, fibrils or ribbons prior to uptake assessment analysis (Fig. 4). Using flow cytometry analysis, we found that microglia took up the different forms of α-syn as soon as they were exposed to them; however, α-syn monomers and distinct assemblies were taken up to a different extent. While about 10% of microglia had taken up α-syn monomers (Fig. 4 A) and oligomers (Fig. 4 B), around 90% of the cells were immunopositive to fibrils (Fig. 4 C) and ribbons (Fig. 4 D) after 5 min of exposure. At time 15 min, 64 and 75% of microglia had incorporated α-syn monomers and oligomers, respectively, while 98% of cells contained fibrils or ribbons. The uptake of α-syn was blocked by the actin polymerization inhibitor cytochalasin D (CytD) in all cases indicating active α-syn phagocytosis by microglia. The engulfment of BSA was performed in parallel as a phagocytosis and degradation control (Fig. S6 A-D). Immunocytochemical analysis of microglia exposed to the different α-syn forms revealed limited internalization of monomers and oligomers as compared to massive uptake of fibrils and ribbons (Fig. 4 E, Fig. S6 E).

To determine whether microglia process α-syn after phagocytosis, we allowed microglia to take up monomers, oligomers, fibrils or ribbons for 15 min and then washed the cells twice with warm PBS and further incubated them for 24 hrs in fresh α-syn-free culture medium. We found that about 50% of all the exogenously applied α-syn monomers and different assemblies remained inside microglia after 24 hrs (Fig. 4 F). Consistently, immune staining of microglia exposed to α-syn oligomers, fibrils or ribbons exhibited aggregates after allowing degradation for 24 hrs (Fig. S6 F) that were largely co-localized to lysosomes (Fig. 4 G-H).

Several studies have shown that cytokines, including NLRP3 inflammasome-derived IL-1β impair β-amyloid uptake (39). In keeping with this, suppression of inflammatory cytokine production resets microglial phagocytosis capacity in the APP/PS1 AD mouse model. To test whether NLRP3 inflammasome activity and the resulting IL-1β release play a similar role in α-syn phagocytosis, the latter was analysed in WT microglia, WT microglia treated with the NLRP3 inflammasome inhibitor CRID3 and NLRP3-knockout microglia (Fig. 5). FACS analysis revealed that α-syn monomers (Fig. 5 A) and oligomers (Fig. 5 B) were engulfed to a significantly greater extent by WT microglia treated with the NLRP3 inflammasome inhibitor CRID3 or NLRP3-knockout microglia compared to WT cells, whereas NLRP3 inhibition or deficiency did not change the engulfment of fibrils (Fig. 5 C) and ribbons (Fig. 5 D). Interestingly, those α-syn monomers and oligomers were previously shown to activate the NLRP3 inflammasome even under basal conditions (Fig. 1). A similar NLRP3-dependent engulfment behaviour was found in microglia exposed to BSA (Fig. S6 D). By expressing the degradation as a function of what was phagocytosed, we found that the degradation of α-syn monomers (Fig. 5 E) was unaffected, while the degradation of oligomers was largely improved

415 in cells deficient for a functional NLRP3 inflammasome (Fig. 5 F). Also, the degradation of α-
416 syn fibrils did not change in WT or NLRP3-deficient microglia (Fig. 5 G), but CRID3-treatment
417 improved the degradation of ribbons, while NLRP3 deficiency did not show any effects (Fig. 5
418 H). Together, these data suggest that there is an inverse relation between microglial NLRP3
419 inflammasome activation (Fig. 1) and its negative regulation on oligomeric α-syn uptake and
420 clearance (Fig. 5).

Discussion

Abnormal α-syn accumulations and microglial activation represent key pathological hallmarks of synucleinopathies. Even though α-syn aggregates are first found in neurons, evidences suggest that spreading of pathology will expose such protein aggregates to surrounding microglia. Microglia are responsible for the clearance of misfolded and aggregated proteins from the brain and represent the main drivers of inflammatory processes within the CNS. They are equipped with PRRs which enable them to respond to α-syn aggregates and their activation has been widely observed in PD (40). Once activated, microglia initiate a range of inflammatory responses including the release of immune mediators such as cytokines and complement factors which, once chronically present, collectively contribute to neuronal dysfunction and degeneration. They also initiate response mechanisms for phagocytic clearance of the respective protein aggregates. Since α-syn proteins can adopt distinct conformations with noticeable differences in their aggregation phenotype, this may cause quantitative and qualitative differences in microglial immune response. The aim of this work is to delineate the different response patterns microglia show when exposed to various α-syn assemblies.

Bent out of shape: α-synuclein misfolding and its inflammatory consequences

NLRP3 inflammasome activation by misfolded proteins, has emerged as important mechanism for neurodegeneration (21) and misfolded α-syn has been reported to cause IL-1β release following microglial NLRP3 inflammasome activation (23). The pathological impact of this finding is further supported by the fact that NLRP3 inhibition prevents α-syn-mediated pathology in multiple rodent PD models (23). Native α-syn exists as a monomer however, under pathological conditions, it forms aggregates with different inflammatory features. Most studies have been focussing on the induction of inflammation by various α-syn oligomers and inhomogeneous fibrillar assemblies. None however addressed the possible pro-inflammatory effects of α-syn monomers and homogeneous and structurally distinct fibrillar polymorphs. Due to variable experimental procedures and concentrations used throughout different reports, a direct comparison between the effects of different α-syn forms on NLRP3 inflammasome activation is therefore impossible. For example, it has been demonstrated elsewhere that 10 µM fibrillar α-syn largely upregulated the assembly of the NLRP3 inflammasome complex in primary microglia that were pre-stimulated with 200 ng/ml LPS (23). In contract, another study reported the induction of the NLRP3 inflammasome upon treatment with 3.5 - 7 µg/ml α-syn upon pre-stimulation of primary microglia with 1 µg/ml LPS (41). Comparing those studies, both, the α-syn concentration and the LPS concentration vary greatly and may possibly complicate any interpretation. Most importantly, both reports do not take possible actions of

458 the monomeric form of α-syn and its potential to activate the NLRP3 inflammasome complex
459 into account. We therefore set out to compare structurally well-characterized recombinant α-
460 syn monomers, oligomers and two fibrillar polymorphs, fibrils and ribbons, for their capacity to
461 induce microglial inflammatory activation (Fig. 1 A-I). Compared to both reports mentioned
462 above, we used microglia that were unprimed or primed with a minimal dose of LPS (10 ng/ml)
463 to avoid microglial over-activation and selected an α-syn concentration that was just sufficient
464 to trigger IL-1β secretion (Fig. S1 C).
465 *In vitro,* microglia show no or just minimal activation of the NLRP3 inflammasome and its
466 priming is usually required as first signaling step of activation by inducing the transcription of
467 its components and substrates including NLRP3, the adaptor ASC, pro-caspase-1 and pro-IL-
468 1β. This is usually followed by a secondary posttranscriptional activation step, that leads to the
469 assembly of the inflammasome complex followed by cleavage of its substrates and cytokine
470 release (21, 26). Here, we provide evidence that α-syn monomers and oligomers are able to
471 effectively activate the inflammasome without the requirement of a prior priming step (Fig. 1 L-
472 R). In contrast, α-syn fibrils showed NLRP3 inflammasome assembly and IL-1β release only
473 after initial priming (Fig. 3 A-G), while ribbons did not affect the NLRP3 inflammasome in
474 microglia.
475 Cell priming occurs through ligation of PRRs which usually respond to a relatively restricted
476 ligand spectrum (42). Various receptors have been implicated in binding to and mediating α-
477 syn signalling in microglia including TLR2, MHCII, Fc receptor and fractalkine receptor (43–
478 46). Using TLR neutralization antibodies we found that monomers and oligomers exert their
479 effects on the NLRP3 inflammasome via TLR2 and TLR5 (Fig. 2). Interestingly, neutralization
480 of TLR2 largely blocked the α-syn-mediated NLRP3 protein expression in unprimed microglia,
481 indicating an important role of TLR2 for NLRP3 inflammasome priming (Fig. 2 G). In addition,
482 TLR5 neutralization prevented caspase-1 cleavage in response to α-syn monomers and
483 oligomers (Fig. 2 F). Thus, our data indicate that TLR2 ligation by α-syn monomer and
484 oligomers implement the inflammasome priming step, whereas TLR5 ligation results in the
485 activation of the inflammasome under basal conditions (Fig. 6). A recent screening of TLR
486 expression dynamics in mouse models of neurodegenerative disease including PD and DLB
487 revealed the upregulation of TLR2 (47), resulting in the activation of microglial inflammation
488 (45, 48, 49). Also, increased TLR2 levels have been found in the SNpc of PD patients (50)
489 further suggesting a pathogenetic role of TLR2 in synucleinopathies. In contrast, TLR5 has not
490 yet been described as a PRR involved in microglial activation by α-syn, this PRR is rather
491 known to be activated by flagellin, a monomer present on the outer cell wall of gram-negative
492 flagella bacteria. While it remains unknown whether flagellin and α-syn monomers and
493 oligomers share a similar TLR recognition site our data provide the first insights into TLR5-

mediated inflammatory activation mechanisms by which α-syn monomers and oligomers prime and activate the NLRP3 inflammasome.

The inverse relation between the NLRP3 inflammasome and α-synuclein clearance

Effective microglial clearance of misfolded and aggregated proteins may play an important role in neurodegenerative disease. α-syn has been shown to be released from neurons and are detectable in biological fluids including plasma and CSF (51, 52), as well as in conditioned media of α-syn expressing neurons (53). Microglia are the main cell type responsible for the uptake and degradation of misfolded or aggregated proteins within the CNS thereby avoiding the spreading of pathology between neighbouring neurons. We therefore assessed the efficacy of microglial uptake and degradation of the aforementioned α-syn species. Microglia quickly internalized the protein in an assembly- and time-dependent manner (Fig. 4), but seemed to fail to fully degrade their cargo (Fig. 5) resulting in the accumulation of internalized α-syn aggregates (Fig. S6 E-F). Several studies provide evidence for impaired clearance mechanisms in PD leading to the idea that α-syn can block its own clearance (54, 55). Alternatively, the microglial activation state may alter its intracellular capacity to effectively degrade the taken-up protein aggregates (56). In response to persistent neurodegeneration, microglia adopt a chronically activated phenotype resulting in the sustained release of cytokines, including IL-1β, that have been found to impair its own clearance functions (57). We therefore analysed the impact of NLRP3 inflammasome inhibition by CRID3 and NLRP3 depletion on the phagocytic and degrading capacity of microglia. A large increase in oligomeric α-syn phagocytosis was found in CRID3-treated WT or NLRP3-knockout microglia (Fig. 5 B). Interestingly we showed that oligomeric α-syn has the potential to activate the inflammasome (Fig. 1), suggesting that NLRP3 inflammasome activation deteriorates microglial phagocytosis (58). In addition, degradation experiments revealed that NLRP3 deficiency substantially induce the depletion of oligomeric α-syn (Fig. 5 B, F). Monomeric α-syn uptake was barely increased in NLRP3 deficient cells (Fig. 5 A), whereas its degradation did not show any NLRP3 dependency (Fig. 5 E). In contrast, uptake and degradation of fibrils and ribbons did not show NLRP3 dependency (Fig. 5).

Taken together, we provide first evidence that α-syn monomers rather than oligomers or fibrillar polymorphs largely induce microglial NLRP3 inflammasome activation. Both, α-syn monomers and, to a lower extent, oligomers had the potential to prime and activate the NLRP3 inflammasome via TLR2 and TLR5 ligation without the requirement of an initial inflammogen (LPS) treatment. Activation of the NLRP3 inflammasome compromised α-syn clearance capacity (Fig. 6). Likewise, NLRP3 inflammasome inhibition or NLRP3 depletion improved α-syn phagocytosis and degradation of α-syn monomers and oligomers. These findings highlight

the potential of targeting the NLRP3 inflammasome or related intracellular signalling mechanisms to control excessive cytokine release mediated by α-syn monomers even before the development of fibrillar complexes.

Acknowledgements

We thank the DZNE light microscope facility (LMF) for providing microscopes and advice and the DZNE Image and Data Analysis Facility (IDAF) for providing analysis computers, software and advice.

Funding

This work was funded by the EC Joint Program on Neurodegenerative Diseases (JPND-SYNACTION-ANR-15-JPWG-0012-03) and by the Deutsche Forschungsgemeinschaft (DFG, German Research Foundation) under Germany's Excellence Strategy - EXC2151 – 390873048. HS received funding's from the Gemeinnützige Hertie Stiftung under the Hertie Network of excellence in clinical neuroscience. RM and LB were supported by the Centre National de la Recherche, the EC Joint Programme on Neurodegenerative Diseases (JPND-SYNACTION-ANR-15-JPWG-0012-03 and TransPath-ND-ANR-17-JPCD-0002-02) and the Fondation Pour La Recherche Médicale (contract DEQ. 20160334896).

Author Contributions

H.S. and M.T.H. designed all experiments; H.S. performed experiments and analysed data with assistance of A.G., S.S. and M.T.H.; L.B. and R.M. generated and characterized all α-synuclein assemblies and provided advice; E.L. provided chemical compounds; H.S. and M.T.H. wrote the manuscript with input from all co-authors.

Disclosures

Michael T. Heneka serves as an advisory board member at IFM Therapeutics, Alector and Tiaki. He received honoraria for oral presentations from Novartis, Roche and Biogen. The other authors declare that there is no conflict of interest with regard to the experimental part of this study.

559 **References**

560 1. Shahmoradian, S. H., A. J. Lewis, C. Genoud, J. Hench, T. E. Moors, P. P. Navarro, D. Castaño-Díez,
561 G. Schweighauser, A. Graff-Meyer, K. N. Goldie, R. Sütterlin, E. Huisman, A. Ingrassia, Y. de Gier, A.
562 J. M. Rozemuller, J. Wang, A. D. Paepe, J. Erny, A. Staempfli, J. Hoernschemeyer, F. Großerüschkamp,
563 D. Niedieker, S. F. El-Mashtoly, M. Quadri, W. F. J. Van IJcken, V. Bonifati, K. Gerwert, B. Bohrmann,
564 S. Frank, M. Britschgi, H. Stahlberg, W. D. J. Van de Berg, and M. E. Lauer. 2019. Lewy pathology in
565 Parkinson's disease consists of crowded organelles and lipid membranes. *Nat. Neurosci.* 22: 1099–
566 1109.

567 2. Spillantini, M. G., M. L. Schmidt, V. M.-Y. Lee, J. Q. Trojanowski, R. Jakes, and M. Goedert. 1997. α-
568 Synuclein in Lewy bodies. *Nature* 388: 839–840.

569 3. Weinreb, P. H., W. Zhen, A. W. Poon, K. A. Conway, and P. T. Lansbury. 1996. NACP, A Protein
570 Implicated in Alzheimer's Disease and Learning, Is Natively Unfolded †. *Biochemistry* 35: 13709–13715.

571 4. Shrivastava, A. N., V. Redeker, N. Fritz, L. Pieri, L. G. Almeida, M. Spolidoro, T. Liebmann, L. Bousset,
572 M. Renner, C. Lena, A. Aperia, R. Melki, and A. Triller. 2015. Alpha-synuclein assemblies sequester
573 neuronal 3-Na+/K+-ATPase and impair Na+ gradient. *EMBO J.* 34: 2408–2423.

574 5. DeWitt, D. C., and E. Rhoades. 2013. α-Synuclein Can Inhibit SNARE-Mediated Vesicle Fusion through
575 Direct Interactions with Lipid Bilayers. *Biochemistry* 52: 2385–2387.

576 6. Faustini, G., F. Bono, A. Valerio, M. Pizzi, P. Spano, and A. Bellucci. 2017. Mitochondria and α-
577 Synuclein: Friends or Foes in the Pathogenesis of Parkinson's Disease? *Genes* 8: 377.

578 7. Gribaudo, S., P. Tixador, L. Bousset, A. Fenyi, P. Lino, R. Melki, J.-M. Peyrin, and A. L. Perrier. 2019.
579 Propagation of α-Synuclein Strains within Human Reconstructed Neuronal Network. *Stem Cell Rep.* 12:
580 230–244.

581 8. Martínez, J. H., F. Fuentes, V. Vanasco, S. Alvarez, A. Alaimo, A. Cassina, F. Coluccio Leskow, and F.
582 Velazquez. 2018. Alpha-synuclein mitochondrial interaction leads to irreversible translocation and
583 complex I impairment. *Arch. Biochem. Biophys.* 651: 1–12.

584 9. Cooper, A. A. 2006. -Synuclein Blocks ER-Golgi Traffic and Rab1 Rescues Neuron Loss in Parkinson's
585 Models. *Science* 313: 324–328.

586 10. Thayanidhi, N., J. R. Helm, D. C. Nycz, M. Bentley, Y. Liang, and J. C. Hay. 2010. α-Synuclein Delays
587 Endoplasmic Reticulum (ER)-to-Golgi Transport in Mammalian Cells by Antagonizing ER/Golgi
588 SNAREs. *Mol. Biol. Cell* 21: 1850–1863.

589 11. Flavin, W. P., L. Bousset, Z. C. Green, Y. Chu, S. Skarpathiotis, M. J. Chaney, J. H. Kordower, R.
590 Melki, and E. M. Campbell. 2017. Endocytic vesicle rupture is a conserved mechanism of cellular
591 invasion by amyloid proteins. *Acta Neuropathol. (Berl.)* 134: 629–653.

592 12. Martinez-Vicente, M., and M. Vila. 2013. Alpha-synuclein and protein degradation pathways in
593 Parkinson's disease: A pathological feed-back loop. *Exp. Neurol.* 247: 308–313.

594 13. Colonna, M., and O. Butovsky. 2017. Microglia Function in the Central Nervous System During Health
595 and Neurodegeneration. *Annu. Rev. Immunol.* 35: 441–468.

596 14. Heneka, M. T., M. P. Kummer, and E. Latz. 2014. Innate immune activation in neurodegenerative
597 disease. *Nat. Rev. Immunol.* 14: 463–477.

598 15. Croisier, E., L. B. Moran, D. T. Dexter, R. K. B. Pearce, and M. B. Graeber. 2005. Microglial
599 inflammation in the parkinsonian substantia nigra: relationship to alpha-synuclein deposition. *J.*
600 *Neuroinflammation* 2: 14.

601 16. Gerhard, A., N. Pavese, G. Hotton, F. Turkheimer, M. Es, A. Hammers, K. Eggert, W. Oertel, R. B.
602 Banati, and D. J. Brooks. 2006. In vivo imaging of microglial activation with [11C](R)-PK11195 PET in
603 idiopathic Parkinson's disease. *Neurobiol. Dis.* 21: 404–412.

604 17. McGeer, P. L., S. Itagaki, B. E. Boyes, and E. G. McGeer. 1988. Reactive microglia are positive for
605 HLA-DR in the substantia nigra of Parkinson's and Alzheimer's disease brains. *Neurology* 38: 1285–
606 1291.

607 18. Allan, S. M., P. J. Tyrrell, and N. J. Rothwell. 2005. Interleukin-1 and neuronal injury. *Nat. Rev.*
608 *Immunol.* 5: 629–640.

609 19. Lamkanfi, M., and V. M. Dixit. 2012. Inflammasomes and Their Roles in Health and Disease. *Annu.*
610 *Rev. Cell Dev. Biol.* 28: 137–161.

611 20. Codolo, G., N. Plotegher, T. Pozzobon, M. Brucale, I. Tessari, L. Bubacco, and M. de Bernard. 2013.

612 Triggering of inflammasome by aggregated α-synuclein, an inflammatory response in synucleinopathies.
613 *PloS One* 8: e55375.

614 21. Heneka, M. T., R. M. McManus, and E. Latz. 2018. Inflammasome signalling in brain function and
615 neurodegenerative disease. *Nat. Rev. Neurosci.* 19: 610–621.

616 22. Wang, S., Y.-H. Yuan, N.-H. Chen, and H.-B. Wang. 2019. The mechanisms of NLRP3
617 inflammasome/pyroptosis activation and their role in Parkinson's disease. *Int. Immunopharmacol.* 67:
618 458–464.

619 23. Gordon, R., E. A. Albornoz, D. C. Christie, M. R. Langley, V. Kumar, S. Mantovani, A. A. B. Robertson,
620 M. S. Butler, D. B. Rowe, L. A. O'Neill, A. G. Kanthasamy, K. Schroder, M. A. Cooper, and T. M.
621 Woodruff. 2018. Inflammasome inhibition prevents α-synuclein pathology and dopaminergic
622 neurodegeneration in mice. *Sci. Transl. Med.* 10.

623 24. Liu, X., and N. Quan. 2018. Microglia and CNS Interleukin-1: Beyond Immunological Concepts. *Front.*
624 *Neurol.* 9: 8.

625 25. Takeuchi, O., and S. Akira. 2010. Pattern Recognition Receptors and Inflammation. *Cell* 140: 805–
626 820.

627 26. Broz, P., and V. M. Dixit. 2016. Inflammasomes: mechanism of assembly, regulation and signalling.
628 *Nat. Rev. Immunol.* 16: 407–420.

629 27. Guo, H., J. B. Callaway, and J. P.-Y. Ting. 2015. Inflammasomes: mechanism of action, role in disease,
630 and therapeutics. *Nat. Med.* 21: 677–687.

631 28. Christgen, S., D. E. Place, and T.-D. Kanneganti. 2020. Toward targeting inflammasomes: insights into
632 their regulation and activation. *Cell Res.* 30: 315–327.

633 29. Bousset, L., L. Pieri, G. Ruiz-Arlandis, J. Gath, P. H. Jensen, B. Habenstein, K. Madiona, V. Olieric, A.
634 Böckmann, and B. H. Meier. 2013. Structural and functional characterization of two alpha-synuclein
635 strains. *Nat. Commun.* 4.

636 30. Peelaerts, W., L. Bousset, A. Van der Perren, A. Moskalyuk, R. Pulizzi, M. Giugliano, C. Van den
637 Haute, R. Melki, and V. Baekelandt. 2015. alpha-Synuclein strains cause distinct synucleinopathies after
638 local and systemic administration. *Nature* 522: 340–344.

639 31. Giulian, D., and T. J. Baker. 1986. Characterization of ameboid microglia isolated from developing
640 mammalian brain. *J. Neurosci.* 6: 2163–2178.

641 32. Ghee, M., R. Melki, N. Michot, and J. Mallet. 2005. PA700, the regulatory complex of the 26S
642 proteasome, interferes with α-synuclein assembly. *FEBS J.* 272: 4023–4033.

643 33. Jakobs, C., E. Bartok, A. Kubarenko, F. Bauernfeind, and V. Hornung. 2013. Immunoblotting for active
644 caspase-1. *Inflammasome Methods Protoc.* 103–115.

645 34. Pieri, L., K. Madiona, and R. Melki. 2016. Structural and functional properties of prefibrillar α-synuclein
646 oligomers. *Sci. Rep.* 6: 1–15.

647 35. Cremades, N., S. Chen, and C. Dobson. 2017. Structural characteristics of α-synuclein oligomers. *Int.*
648 *Rev. Cell Mol. Biol.* 329: 79–143.

649 36. Lashuel, H. A., B. M. Petre, J. Wall, M. Simon, R. J. Nowak, T. Walz, and P. T. Lansbury Jr. 2002. α-
650 Synuclein, especially the Parkinson's disease-associated mutants, forms pore-like annular and tubular
651 protofibrils. *J. Mol. Biol.* 322: 1089–1102.

652 37. Shrivastava, A. N., L. Bousset, M. Renner, V. Redeker, J. Savistchenko, A. Triller, and R. Melki. 2020.
653 Differential membrane binding and seeding of distinct α-synuclein fibrillar polymorphs. *Biophys. J.* 118:
654 1301–1320.

655 38. Fernandes-Alnemri, T., J. Wu, J.-W. Yu, P. Datta, B. Miller, W. Jankowski, S. Rosenberg, J. Zhang,
656 and E. S. Alnemri. 2007. The pyroptosome: a supramolecular assembly of ASC dimers mediating
657 inflammatory cell death via caspase-1 activation. *Cell Death Differ.* 14: 1590–1604.

658 39. Heneka, M. T., M. P. Kummer, A. Stutz, A. Delekate, S. Schwartz, A. Vieira-Saecker, A. Griep, D. Axt,
659 A. Remus, T.-C. Tzeng, E. Gelpi, A. Halle, M. Korte, E. Latz, and D. T. Golenbock. 2013. NLRP3 is
660 activated in Alzheimer's disease and contributes to pathology in APP/PS1 mice. *Nature* 493: 674–678.

661 40. Lecours, C., M. Bordeleau, L. Cantin, M. Parent, T. D. Paolo, and M.-È. Tremblay. 2018. Microglial
662 Implication in Parkinson's Disease: Loss of Beneficial Physiological Roles or Gain of Inflammatory
663 Functions? *Front. Cell. Neurosci.* 12: 282.

664 41. Panicker, N., S. Sarkar, D. S. Harischandra, M. Neal, T.-I. Kam, H. Jin, H. Saminathan, M. Langley, A.

665 Charli, M. Samidurai, D. Rokad, S. Ghaisas, O. Pletnikova, V. L. Dawson, T. M. Dawson, V. Anantharam,
666 A. G. Kanthasamy, and A. Kanthasamy. 2019. Fyn kinase regulates misfolded α-synuclein uptake and
667 NLRP3 inflammasome activation in microglia. *J. Exp. Med.* 216: 1411–1430.

668 42. Akira, S., S. Uematsu, and O. Takeuchi. 2006. Pathogen Recognition and Innate Immunity. *Cell* 124:
669 783–801.

670 43. Cao, S., D. G. Standaert, and A. S. Harms. 2012. The gamma chain subunit of Fc receptors is required
671 for alpha-synuclein-induced pro-inflammatory signaling in microglia. *J. Neuroinflammation* 9: 259.

672 44. Harms, A. S., S. Cao, A. L. Rowse, A. D. Thome, X. Li, L. R. Mangieri, R. Q. Cron, J. J. Shacka, C.
673 Raman, and D. G. Standaert. 2013. MHCII Is Required for -Synuclein-Induced Activation of Microglia,
674 CD4 T Cell Proliferation, and Dopaminergic Neurodegeneration. *J. Neurosci.* 33: 9592–9600.

675 45. Kim, C., D.-H. Ho, J.-E. Suk, S. You, S. Michael, J. Kang, S. Joong Lee, E. Masliah, D. Hwang, H.-J.
676 Lee, and S.-J. Lee. 2013. Neuron-released oligomeric α-synuclein is an endogenous agonist of TLR2
677 for paracrine activation of microglia. *Nat. Commun.* 4.

678 46. Thome, A. D., D. G. Standaert, and A. S. Harms. 2015. Fractalkine Signaling Regulates the
679 Inflammatory Response in an α-Synuclein Model of Parkinson Disease. *PLOS ONE* 10: e0140566.

680 47. Letiembre, M., Y. Liu, S. Walter, W. Hao, T. Pfander, A. Wrede, W. Schulz-Schaeffer, and K.
681 Fassbender. 2009. Screening of innate immune receptors in neurodegenerative diseases: A similar
682 pattern. *Neurobiol. Aging* 30: 759–768.

683 48. Béraud, D., M. Twomey, B. Bloom, A. Mittereder, V. Ton, K. Neitzke, S. Chasovskikh, T. R. Mhyre, and
684 K. A. Maguire-Zeiss. 2011. α-Synuclein Alters Toll-Like Receptor Expression. *Front. Neurosci.* 5.

685 49. Gustot, A., J. I. Gallea, R. Sarroukh, M. S. Celej, J.-M. Ruysschaert, and V. Raussens. 2015. Amyloid
686 fibrils are the molecular trigger of inflammation in Parkinson's disease. *Biochem. J.* 471: 323–333.

687 50. Doorn, K. J., T. Moors, B. Drukarch, W. D. van de Berg, P. J. Lucassen, and A.-M. van Dam. 2014.
688 Microglial phenotypes and toll-like receptor 2 in the substantia nigra and hippocampus of incidental Lewy
689 body disease cases and Parkinson's disease patients. *Acta Neuropathol. Commun.* 2: 90.

690 51. El-Agnaf, O. M. A., S. A. Salem, K. E. Paleologou, L. J. Cooper, N. J. Fullwood, M. J. Gibson, M. D.
691 Curran, J. A. Court, D. M. A. Mann, S.-I. Ikeda, M. R. Cookson, J. Hardy, and D. Allsop. 2003. α-
692 Synuclein implicated in Parkinson's disease is present in extracellular biological fluids, including human
693 plasma. *FASEB J.* 17: 1945–1947.

694 52. Mollenhauer, B., J. J. Locascio, W. Schulz-Schaeffer, F. Sixel-Döring, C. Trenkwalder, and M. G.
695 Schlossmacher. 2011. α-Synuclein and tau concentrations in cerebrospinal fluid of patients presenting
696 with parkinsonism: a cohort study. *Lancet Neurol.* 10: 230–240.

697 53. Emmanouilidou, E., K. Melachroinou, T. Roumeliotis, S. D. Garbis, M. Ntzouni, L. H. Margaritis, L.
698 Stefanis, and K. Vekrellis. 2010. Cell-Produced -Synuclein Is Secreted in a Calcium-Dependent Manner
699 by Exosomes and Impacts Neuronal Survival. *J. Neurosci.* 30: 6838–6851.

700 54. Cuervo, A. M., L. Stefanis, R. Fredenburg, P. T. Lansbury, and D. Sulzer. 2004. Impaired degradation
701 of mutant α-synuclein by chaperone-mediated autophagy. *Science* 305: 1292–1295.

702 55. Snyder, H., K. Mensah, C. Theisler, J. Lee, A. Matouschek, and B. Wolozin. 2003. Aggregated and
703 monomeric α-synuclein bind to the S6′ proteasomal protein and inhibit proteasomal function. *J. Biol.*
704 *Chem.* 278: 11753–11759.

705 56. Lee, H.-J., J.-E. Suk, E.-J. Bae, and S.-J. Lee. 2008. Clearance and deposition of extracellular α-
706 synuclein aggregates in microglia. *Biochem. Biophys. Res. Commun.* 372: 423–428.

707 57. Hickman, S. E., E. K. Allison, and J. El Khoury. 2008. Microglial Dysfunction and Defective -Amyloid
708 Clearance Pathways in Aging Alzheimer's Disease Mice. *J. Neurosci.* 28: 8354–8360.

709 58. Jin, L., S. Batra, and S. Jeyaseelan. 2017. Deletion of Nlrp3 augments survival during polymicrobial
710 sepsis by decreasing autophagy and enhancing phagocytosis. *J. Immunol.* 198: 1253–1262.

711

712

Figure Legends

Figure 1

Different forms of α-syn prime and activate the NLRP3 inflammasome under basal conditions.

(A) Schematic drawing of the α-syn species used throughout this study. **(B-I)** Characterization of the α-syn species used throughout this study. **(B)** The monomeric nature of α-syn was assessed by analytical ultracentrifugation. **(C)** The assembly of monomeric α-syn (100 μM) into the fibrillar polymorphs Fibrils (red) and Ribbons (green) was monitored in triplicate using Thioflavin T binding as this assay shows the lag phase is short and the fluorescence at steady state high for the polymorph fibrils as compared to that of the polymorph ribbons. **(D-H)** Electron micrographs of oligomeric and fibrillar α-syn species after negative staining with Uranyl acetate (1%). **(D)** On fibrillar assembly pathway oligomeric α-syn purified through a Superose 6 column. **(E-F)** The fibrillar polymorph fibrils before and after fragmentation into particles with an average size 40 nm, respectively. **(G-H)** The fibrillar polymorph ribbons before and after fragmentation into particles with an average size 40 nm, respectively. **(I-K)** Proteolytic patterns upon exposure to Proteinase K of the α-syn oligomers **(I)**, and the fibrillar polymorphs Fibrils **(J)** and Ribbons **(K)** after SDS-PAGE and Commassie blue staining. The arrowheads on the right point to bands that distinguish the polymorph Fibrils from the polymorph Ribbons. **(L-M)** IL-1β levels in conditioned medium of primary microglia treated for 6 hrs **(L)** or 24 hrs **(M)** with 2 μM α-syn monomers, oligomers, fibrils, and ribbons. BSA was used as protein control. (for A: n=3; for B: n=7-10 independent experiments with triplicate treatments for all conditions). **(N)** Immunoblot of microglia cell lysates and supernatants exposed to 2 μM α-syn for 24 hrs, stained for caspase-1, NLRP3, ASC and α-tubulin. (for lysates: n=7-9; for supernatants: n=5 independent experiments). Quantification of caspase-1 p45 **(O)**, secreted cleaves caspase-1 p20 **(P)**, NLRP3 **(Q)**, and ASC **(R)** of cell lysates and supernatants of microglia exposed for 24 hrs to 2 μM α-syn. All graphs are presented as mean ± SEM and were analysed by one-way ANOVA followed by Tukey's multiple comparison post hoc test (O-R) or Kruskal-Wallis test for nonparametric data (L-M). Levels of significance are: ****p < 0.0001, ***p < 0.001, **p < 0.01, *p < 0.05. Scale bars: 20 μm. See also Fig. S1 and Fig. S3.

Figure 2

Toll-like receptor 2 (TLR2) and TLR5 neutralization suppress α-syn-mediated IL-1β release following NLRP3 inflammasome activation in primary microglia.

(A) Immunoblot analysis and quantification of the expression of MyD88 after exposure to 2 μM α-syn for 24 hrs. (n=3 independent experiments). **(B)** Immunoblot analysis and quantification of the expression of NFκB in microglia cell lysates exposed to 2 μM α-syn for 24 hrs. **(C)** Representative staining with NFκB (magenta) of microglia exposed to α-syn show the translocation of NFκB from the cytoplasm when treated with LPS or α-syn monomers for 24 hrs. Arrows point toward the translocation of NFκB into the nucleus (DAPI, blue). **(D)** Quantification of the translocation of NFκB from the cytosol to the nucleus in microglia exposed for 24 hrs to 2 μM α-syn. IL-1β levels in conditioned medium of unprimed primary microglia treated for 24 hrs with TLR2-, TLR4, and TLR5-neutralizing antibodies or the respective isotype controls in parallel to stimulation with α-syn monomers **(E)**, oligomers **(F)**, fibrils **(G)** and ribbons **(H)**. The baseline release of IL-1β is indicated by the red dashed line for all graphs. (n = 3-4 per group with duplicate or triplicate treatments for all conditions). **(I)** Immunoblot for caspase-1 p45, cleaved caspase-1 p20, NLRP3, ASC and α-tubulin. Quantification of secreted cleaved caspase-1 p20 **(J)** and NLRP3 **(K)** in microglia treated with the different α-syn forms alone (Ø) or in combination with TLR2-, TLR4-, TLR5-neutralizing antibodies or the respective IgG controls. (n=4 independent experiments). All graphs are presented as mean ± SEM and were analysed by one-way ANOVA followed by Tukey's multiple comparison post hoc test. Levels of significance are: ****p < 0.0001, ***p < 0.001, **p < 0.01, *p < 0.05. See also Fig. S2.

Figure 3

Different forms of α-syn activate the NLRP3 inflammasome in LPS-primed microglia.

IL-1β levels in conditioned medium of LPS-primed primary microglia treated for 6 hrs **(A)** or 24 hrs **(B)** with 2 μM α-syn monomers, oligomers, fibrils, and ribbons. BSA was used as protein control. (for A: n=3; for B: n=7-10 independent experiments with triplicate treatments for all conditions). **(C)** Immunoblot of primed microglia cell lysates and supernatants exposed to 2 μM α-syn for 24 hrs, stained for caspase-1, NLRP3, ASC and α-tubulin. (for lysates: n=7-9; for supernatants: n=5 independent experiments). Quantification of caspase-1 p45 **(D)**, secreted cleaves caspase-1 p20 **(E)**, NLRP3 **(F)**, and ASC **(G)** of cell lysates and supernatants of LPS-primed microglia exposed for 24 hrs to 2 μM α-syn. **(H)**

Representative staining with ASC (red) of LPS-primed microglia exposed to α-syn-Atto488 (green) show the formation of ASC specks after 24 hrs. **(I)** Quantification of the number of ASC-speck containing cells. (n=3 independent experiments). **(J)** Co-localization analysis of ASC specks and α-syn after 24 hrs exposure. (n=3 independent experiments). IL-1β levels in conditioned medium of LPS-primed primary microglia treated for 24 hrs with TLR2-neutralizing antibody or the respective isotype control in parallel to stimulation with α-syn monomers **(K)**, oligomers **(L)**, fibrils **(M)** or ribbons **(N)**. The baseline release of IL-1β is indicated by the red dashed line for all graphs. (n = 3-6 per group with duplicate or triplicate treatments for all conditions). All graphs are presented as mean ± SEM and were analysed by one-way ANOVA followed by Tukey's multiple comparison post hoc test (D-I, K-N) or Kruskal-Wallis test for nonparametric data (A, B, J). Levels of significance are: ****p < 0.0001, ***p < 0.001, **p < 0.01, *p < 0.05. Scale bars: 20 μm. See also Fig. S4.

Figure 4

Microglia take up α-syn within minutes but hesitate in its degradation.

Flow cytometric analysis and quantification of the percentage of α-syn-positive cells after exposure to 2 μM monomers **(A)**, oligomers **(B)**, fibrils **(C)**, and ribbons **(D)**. (n=5 independent experiments). Active α-syn uptake was verified by inhibiting the engulfment with the phagocytosis inhibitor cytochalasin D (CytD). **(E)** Representative immunostainings for CD11b-positive microglia (red) containing distinct forms of α-syn-Atto488 (green). DAPI (blue) was used as a counterstain. **(F)** Quantification of the percentage of α-syn degradation after 24h in microglia treated with 2 μM α-syn monomers (grey), oligomers (blue), fibrils (red), or ribbons (green). (n=4 independent experiments with duplicated treatments for all conditions). Representative immunostaining **(G)** for LysoTracker (red) and α-syn-Atto488 (green) and quantification **(H)** of the Lysosome : α-syn co-localization calculated by the Pearson's correlation coefficient. Graphs in (A-D) are presented as mean ± SEM and were analysed by one-way ANOVA followed by Tukey's multiple comparison post hoc test (B-D) or Kruskal-Wallis test for nonparametric data (A). Graphs in F are presented as mean ± SEM and were analysed by an unpaired t-test. Levels of significance are: ****p < 0.0001, ***p < 0.001, **p < 0.01, *p < 0.05. Scale bars: 20 μm. See also Fig. S6.

Figure 5

Microglia take up α-syn monomers and oligomers in a NLRP3 dependent manner.

Quantification and comparison or the relative uptake and degradation of α-syn monomers **(A)**, oligomers **(B)**, fibrils **(C)**, and ribbons **(D)** by WT microglia (filled bars), WT microglia treated with 200 nM of the NLRP3 inhibitor CRID3 (striped bars), and NLRP3-deficient microglia (empty bars). Expression of the degradation as a function of α-syn monomers **(E)**, oligomers **(F)**, fibrils **(G)** and ribbons **(H)** that have been phagocytosed by WT microglia (filled bars), WT microglia treated with 200 nM of the NLRP3 inhibitor CRID3 (striped bars), and NLRP3-deficient microglia (empty bars). (n=6-7 independent experiments). All graphs are presented as mean ± SEM and were analysed by one-way ANOVA followed by Tukey's multiple comparison post hoc test. Levels of significance are: ****p < 0.0001, ***p < 0.001, **p < 0.01, *p < 0.05. See also Fig. S6.

Figure 6

The inverse relationship between microglial NLRP3 inflammasome activation and α-syn clearance.

The schematic was created with BioRender (https://biorender.com). TLR2 ligation by α-syn monomer and oligomers induce the expression of NLRP3, ASC and caspase-1 p45 following translocation of NFκB to the nucleus. Ligation of TLR5 by α-syn monomer and oligomers acts as a "activation" stimulus resulting in the assembly of the NLRP3 inflammasome and the release of IL-1β. Activation of the NLRP3 inflammasome blocks the phagocytosis and degradation of α-syn oligomers, and to a lower extent α-syn monomers, resulting in protein accumulation.

Figure 1

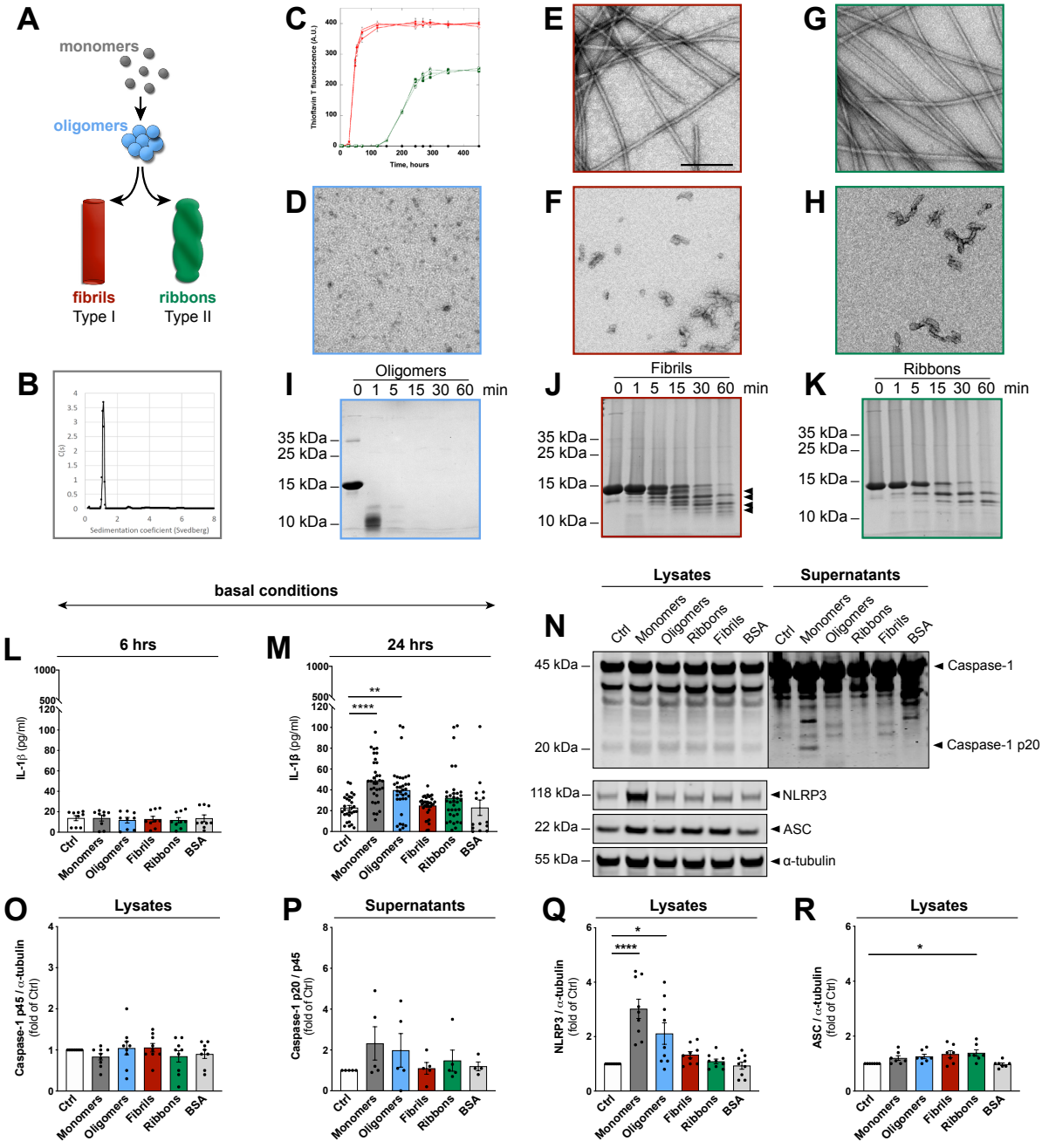
A
monomers
oligomers
fibrils
Type I
ribbons
Type II
B
C
Thioflavin T fluorescence (A.U.)
Time, hours
D
E
F
G
H
I
Oligomers
0 1 5 15 30 60 min
35 kDa
25 kDa
15 kDa
10 kDa
J
Fibrils
0 1 5 15 30 60 min
K
Ribbons
0 1 5 15 30 60 min
basal conditions
L
6 hrs
IL-1β (pg/ml)
M
24 hrs
Ctrl
Monomers
Oligomers
Fibrils
Ribbons
BSA
N
Lysates
Supernatants
45 kDa
20 kDa
Caspase-1
Caspase-1 p20
118 kDa
22 kDa
55 kDa
NLRP3
ASC
α-tubulin
O
Caspase-1 p45 / α-tubulin (fold of Ctrl)
P
Caspase-1 p20 / p45 (fold of Ctrl)
Q
NLRP3 / α-tubulin (fold of Ctrl)
R
ASC / α-tubulin (fold of Ctrl)

822

Figure 2

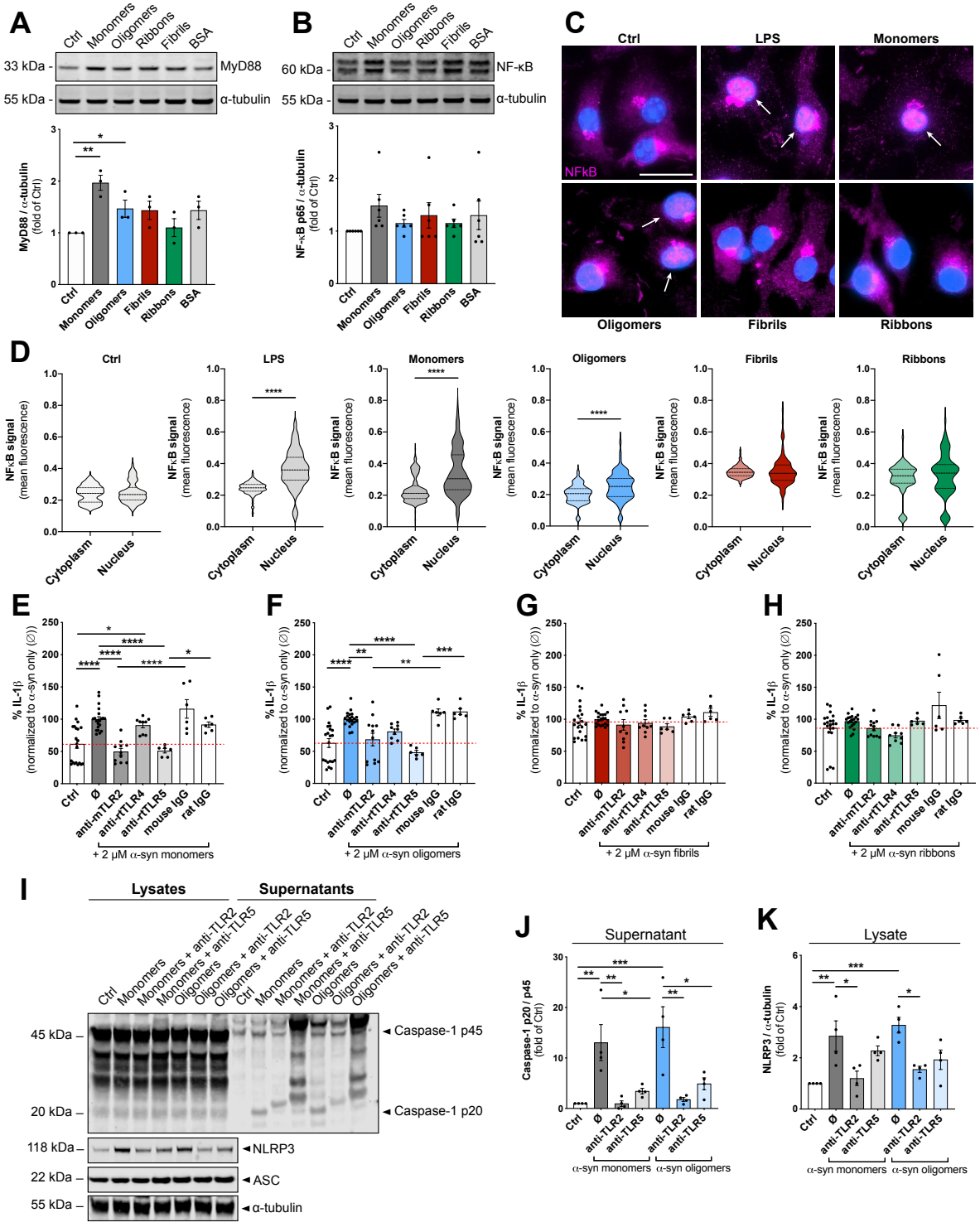
A
Ctrl
Monomers
Oligomers
Ribbons
Fibrils
BSA
33 kDa -
MyD88
55 kDa -
α-tubulin
MyD88 / α-tubulin (fold of Ctrl)
B
60 kDa -
NF-κB
55 kDa -
α-tubulin
NF-κB p65 / α-tubulin (fold of Ctrl)
C
Ctrl
LPS
Monomers
NFkB
Oligomers
Fibrils
Ribbons
D
Ctrl
LPS
Monomers
Oligomers
Fibrils
Ribbons
NFκB signal (mean fluorescence)
Cytoplasm
Nucleus
E
F
G
H
% IL-1β (normalized to α-syn only (∅))
Ctrl
Ø
anti-mTLR2
anti-rtTLR4
anti-rtTLR5
mouse IgG
rat IgG
+ 2 μM α-syn monomers
+ 2 μM α-syn oligomers
+ 2 μM α-syn fibrils
+ 2 μM α-syn ribbons
I
Lysates
Supernatants
Monomers + anti-TLR2
Monomers + anti-TLR5
Oligomers + anti-TLR2
Oligomers + anti-TLR5
45 kDa
20 kDa
118 kDa
22 kDa
55 kDa
Caspase-1 p45
Caspase-1 p20
NLRP3
ASC
α-tubulin
J
Supernatant
Caspase-1 p20 / p45 (fold of Ctrl)
α-syn monomers
α-syn oligomers
K
Lysate
NLRP3 / α-tubulin (fold of Ctrl)

823

Figure 3

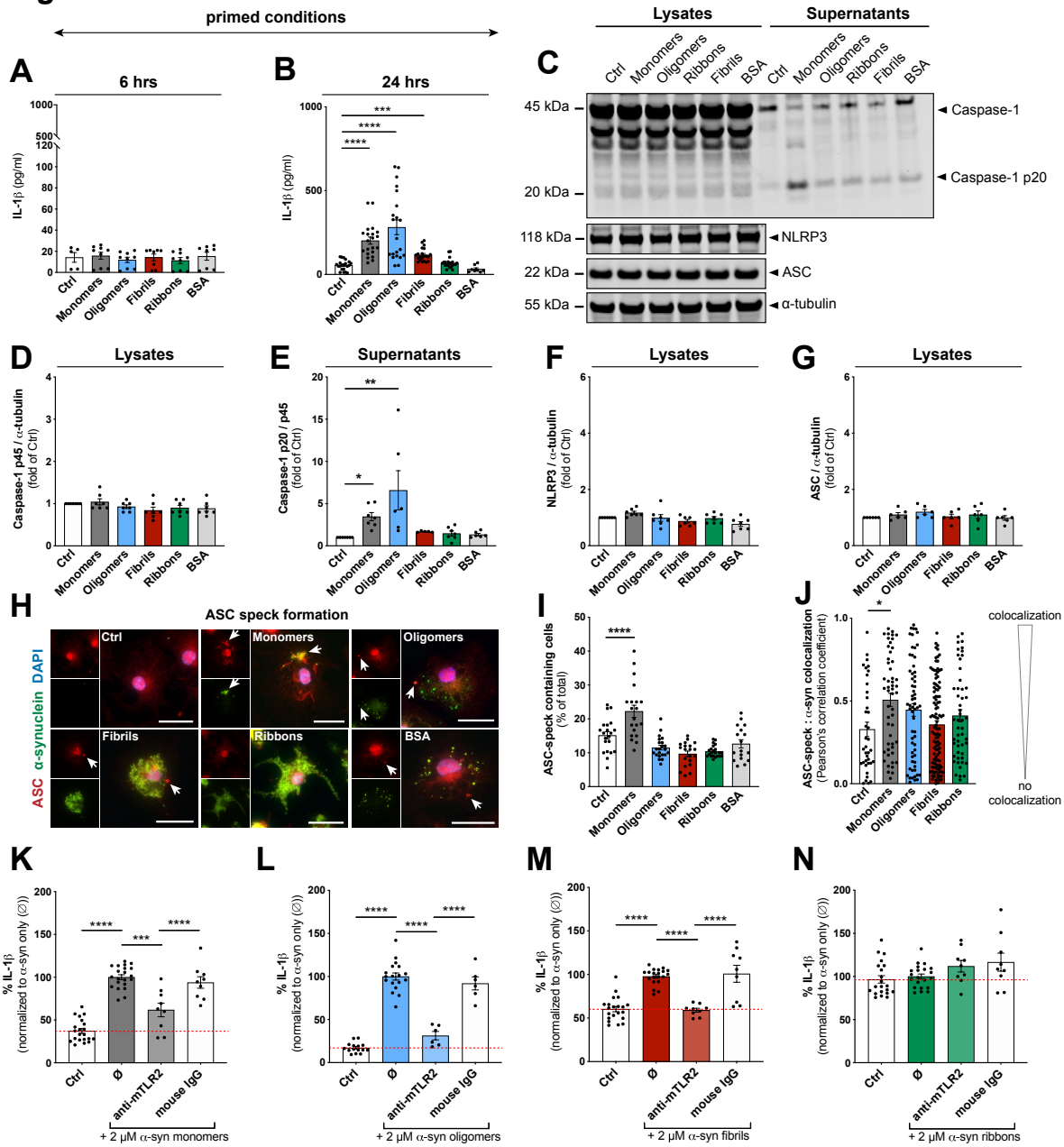
primed conditions
A
6 hrs
IL-1β (pg/ml)
Ctrl
Monomers
Oligomers
Fibrils
Ribbons
BSA
B
24 hrs
C
Lysates
Supernatants
45 kDa
20 kDa
118 kDa
22 kDa
55 kDa
Caspase-1
Caspase-1 p20
NLRP3
ASC
α-tubulin
D
Lysates
Caspase-1 p45 / α-tubulin (fold of Ctrl)
E
Supernatants
Caspase-1 p20 / p45 (fold of Ctrl)
F
Lysates
NLRP3 / α-tubulin (fold of Ctrl)
G
Lysates
ASC / α-tubulin (fold of Ctrl)
H
ASC speck formation
DAPI
α-synuclein
ASC
I
ASC-speck containing cells (% of total)
J
ASC-speck : α-syn colocalization (Pearson's correlation coefficient)
colocalization
no colocalization
K
% IL-1β (normalized to α-syn only (∅))
Ø
anti-mTLR2
mouse IgG
+ 2 μM α-syn monomers
L
+ 2 μM α-syn oligomers
M
+ 2 μM α-syn fibrils
N
+ 2 μM α-syn ribbons

824

Figure 4

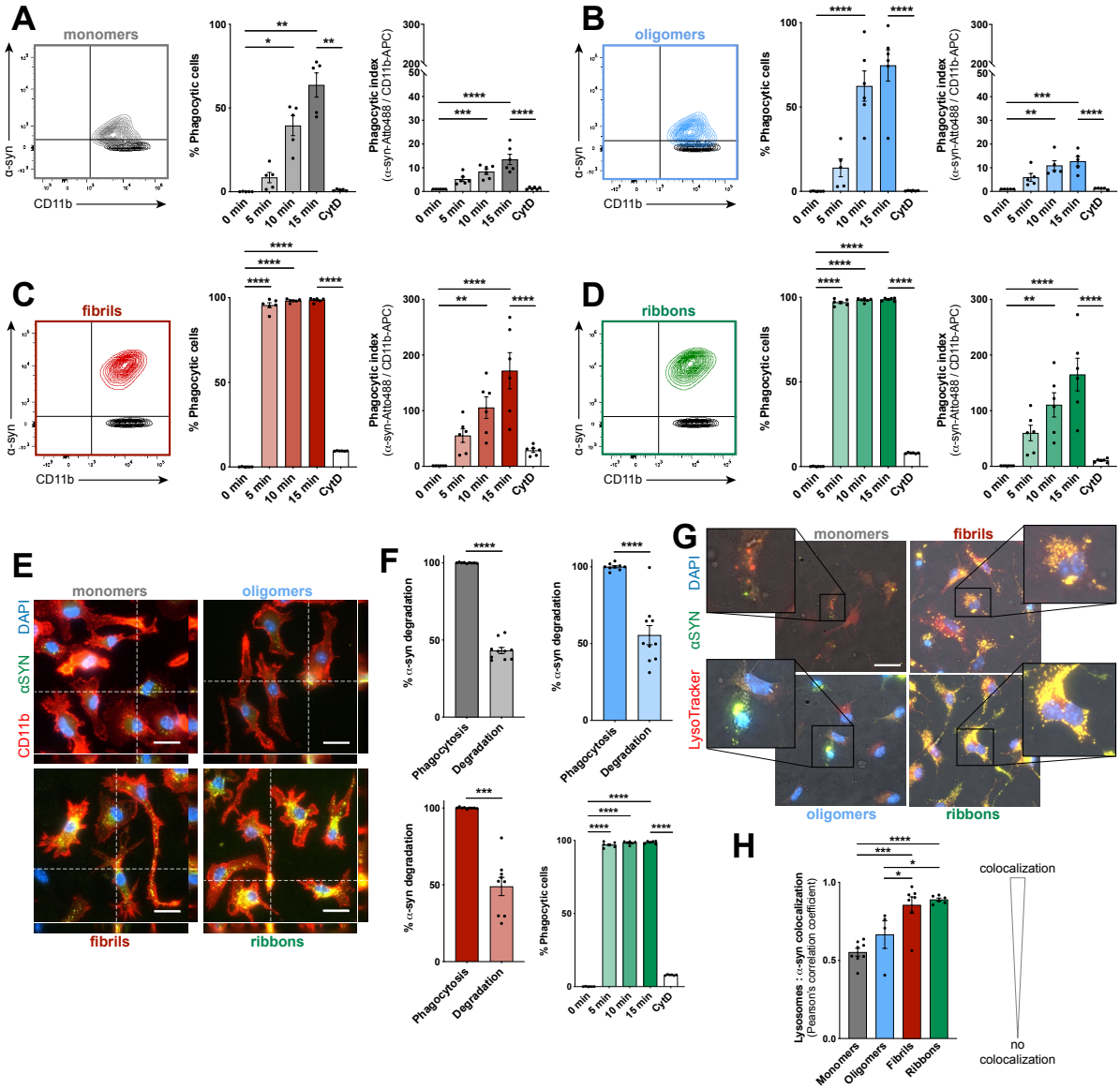
A
monomers
α-syn
CD11b
% Phagocytic cells
Phagocytic index (α-syn-Atto488 / CD11b-APC)
0 min
5 min
10 min
15 min
CytD
B
oligomers
C
fibrils
D
ribbons
E
monomers
oligomers
DAPI
αSYN
CD11b
fibrils
ribbons
F
% α-syn degradation
Phagocytosis
Degradation
% Phagocytic cells
G
monomers
fibrils
DAPI
αSYN
LysoTracker
oligomers
ribbons
H
Lysosomes : α-syn colocalization
(Pearson's correlation coefficient)
Monomers
Oligomers
Fibrils
Ribbons
colocalization
no colocalization

825

Figure 5

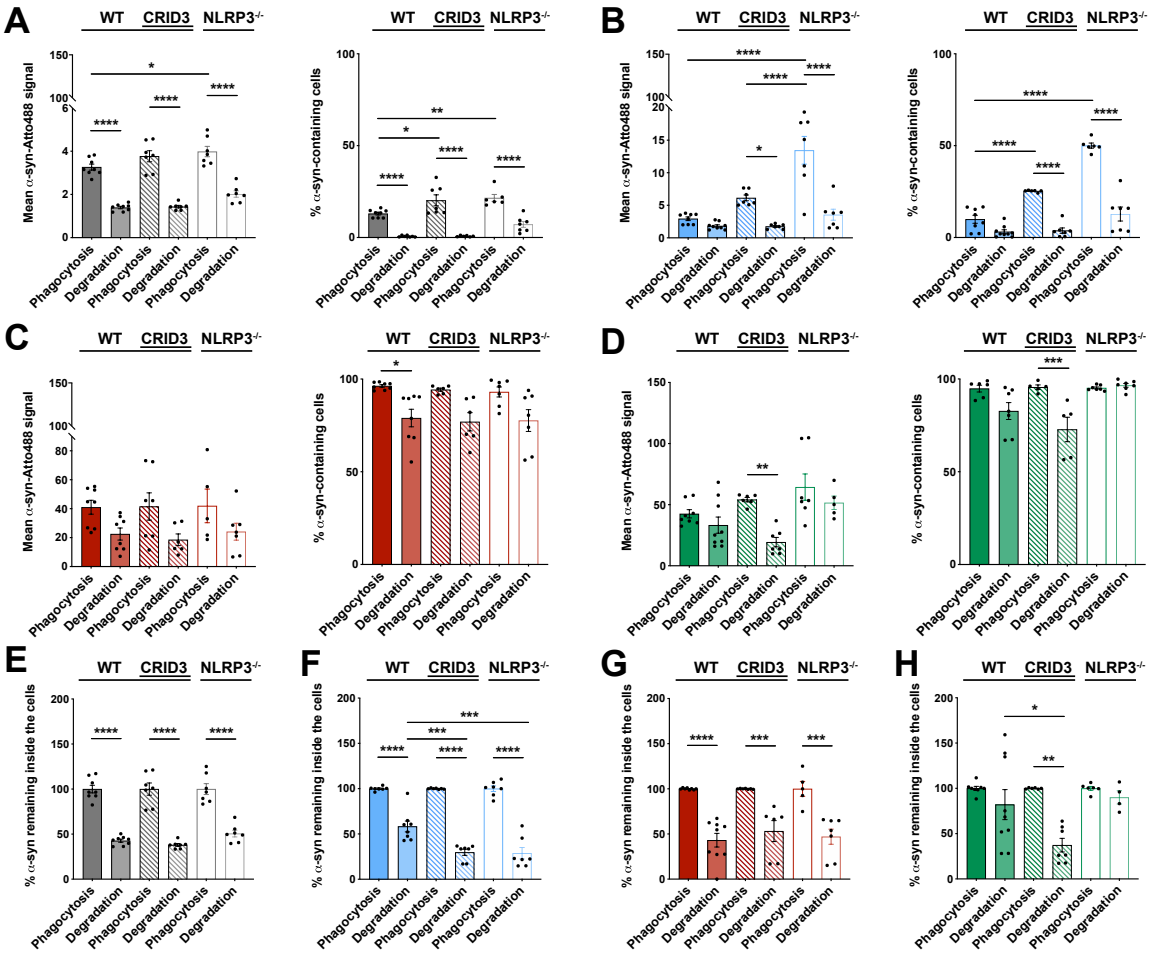
A
B
C
D
E
F
G
H
WT
CRID3
NLRP3-/-
Mean α-syn-Atto488 signal
% α-syn-containing cells
% α-syn remaining inside the cells
Phagocytosis
Degradation

826

Figure 6

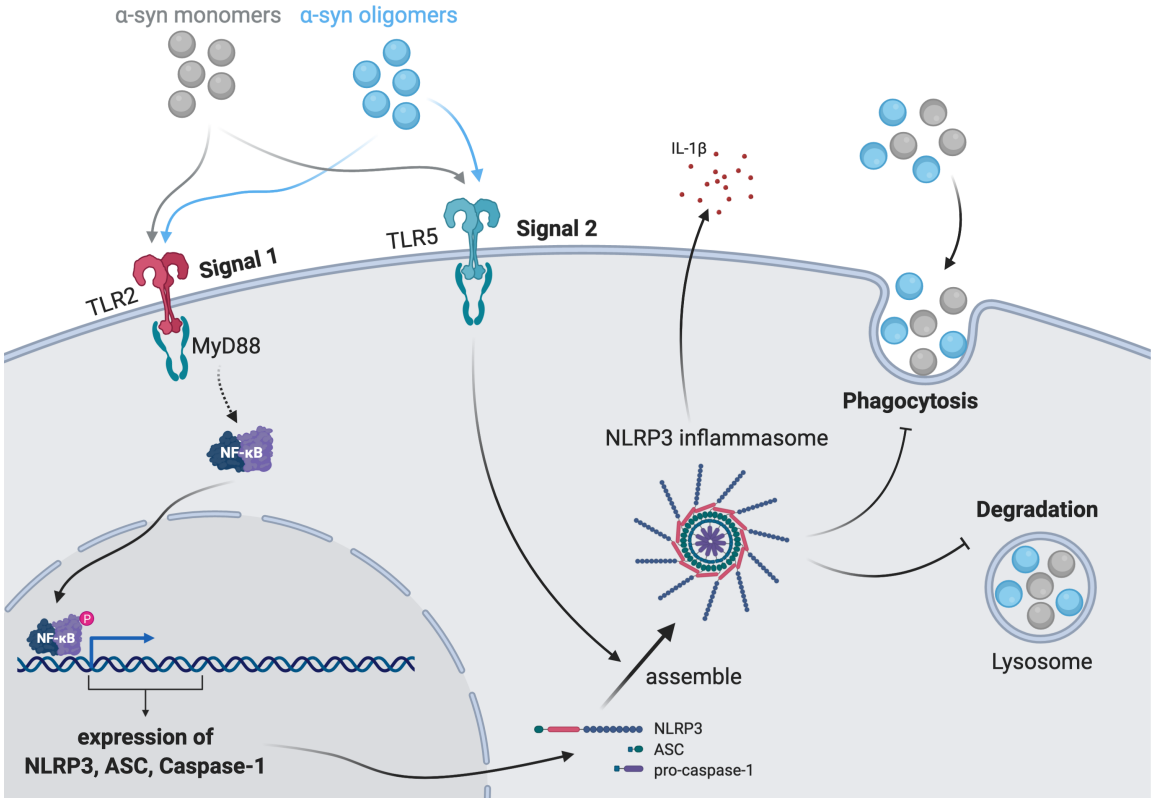
α-syn monomers
α-syn oligomers
TLR2
Signal 1
MyD88
TLR5
Signal 2
IL-1β
Phagocytosis
NLRP3 inflammasome
Degradation
Lysosome
NF-κB
NF-κB
expression of
NLRP3, ASC, Caspase-1
assemble
NLRP3
ASC
pro-caspase-1

827

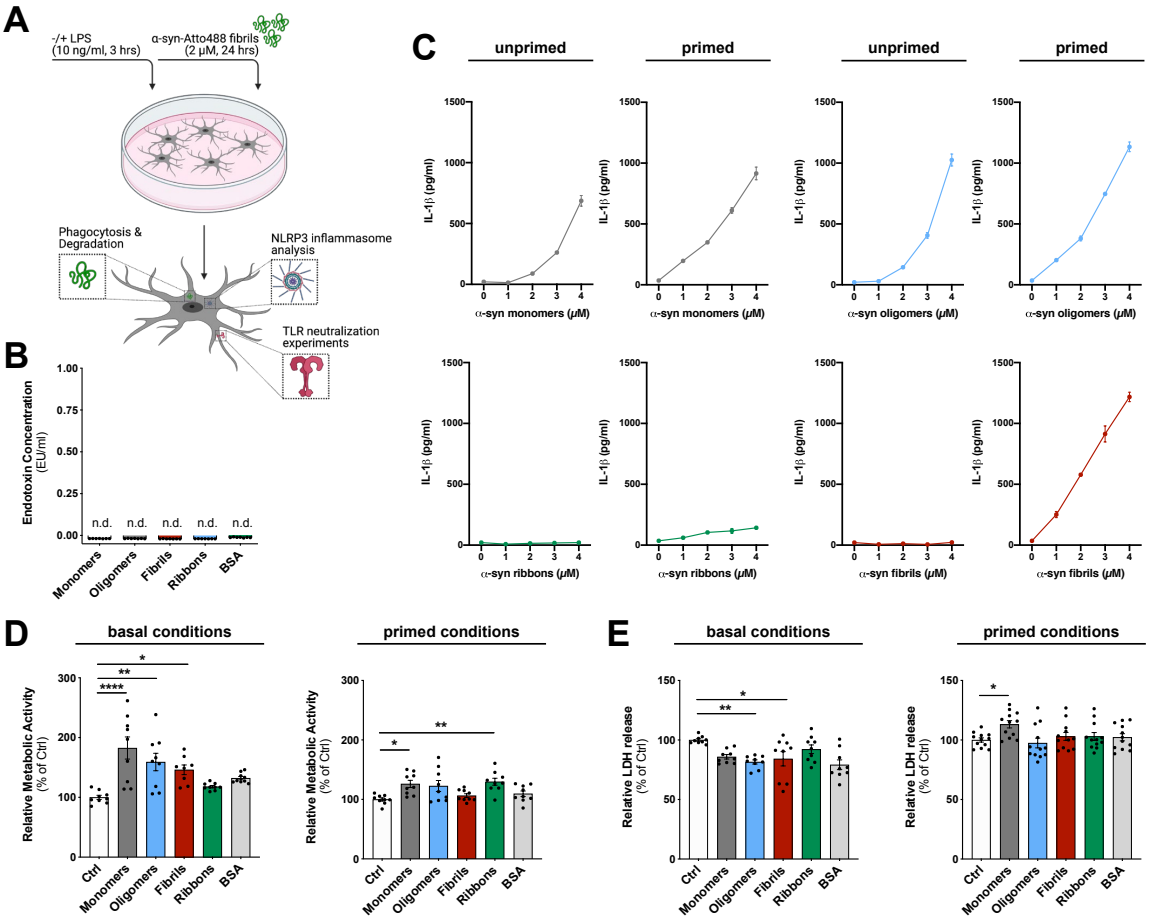

Figure S1

(A) Schematic drawing of the experimental setup used in this study. **(B)** Quantification of the different α-syn forms for endotoxin verify the preparations as endotoxin-free. (n=3 independent experiments with triplicated measurements). **(C)** Quantification of IL-1β levels in conditioned medium of primary microglia treated for 24 hrs with different concentrations of distinct α-syn forms. (n=4 independent experiments with dublicated measurements). Quantification of the relative metabolic activity **(D)** and the relative LDH release **(E)** by microglia treated with 2 µM α-syn under basal conditions or after pre-exposure to LPS. See also Fig. 1. All graphs are presented as mean ± SEM and were analysed by one-way ANOVA followed by Tukey's multiple comparison post hoc test. Levels of significance are: ****p < 0.0001, ***p < 0.001, **p < 0.01, *p < 0.05.

828

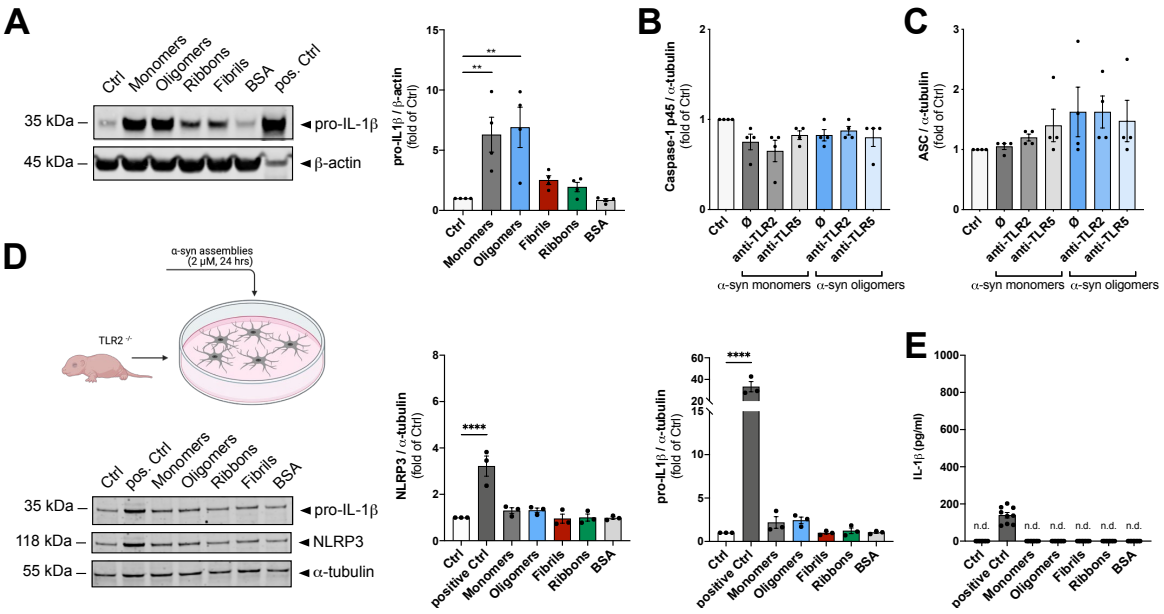

Figure S2

(A) Immunoblot analysis and quantifications of pro-IL1β levels in microglia treated with different α-syn assemblies. Quantification of caspase-1 p45 **(B)** and ASC **(C)** expression upon treatment with TLR2 and TLR5 neutralizing antibodies. (n=4 independent experiments). **(D)** Immunoblot analysis and quantifications of pro-IL1β and NLRP3 levels in microglia derived from TLR2$^{-/-}$ mice treated with different α-syn assemblies. (n=3 independent experiments). **(E)** Quantification of IL-1β levels in conditioned medium of primary microglia derived from TLR2$^{-/-}$ mice treated for 24 hrs with 2 µM distinct α-syn forms and 200 nM CRID3. (n=3 independent experiments with triplicated measurements). See also Fig. 2. All graphs are presented as mean ± SEM and were analysed by one-way ANOVA followed by Tukey's multiple comparison post hoc test **(A, D-E)** or Kruskal-Wallis test for nonparametric data **(B-C)**. Levels of significance are: ****p < 0.0001, ***p < 0.001, **p < 0.01, *p < 0.05.

829

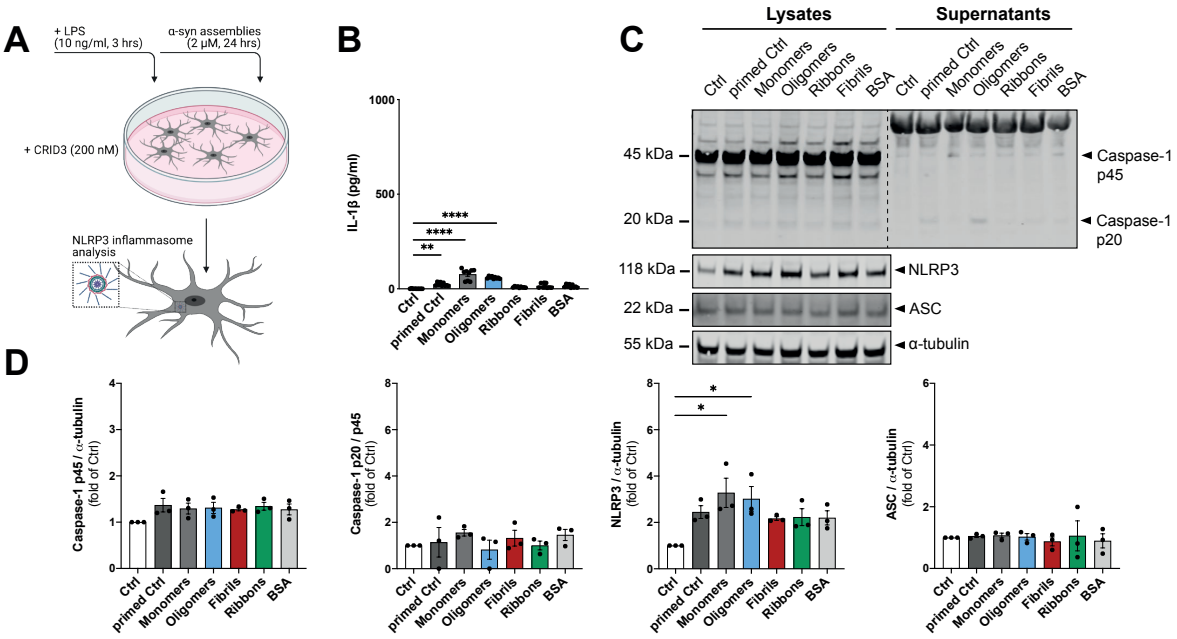

Figure S3
(A) Schematic drawing of the experimental setup used for the following experiments **(B-D)**. **(B)** Quantification of IL-1β levels in conditioned medium of LPS-primed primary microglia treated for 24 hrs with 2 µM distinct α-syn forms and 200 nM CRID3. (n=3 independent experiments with triplicated measurements). **(C-D)** Immunoblot and quantification of primed microglia cell lysates and supernatants exposed to 2 µM α-syn and 200 nM CRID3 for 24 hrs, stained for caspase-1, NLRP3, ASC and α-tubulin. All graphs are presented as mean ± SEM and were analysed by one-way ANOVA followed by Tukey's multiple comparison post hoc test. Levels of significance are: ****p < 0.0001, **p < 0.01, *p < 0.05.

830

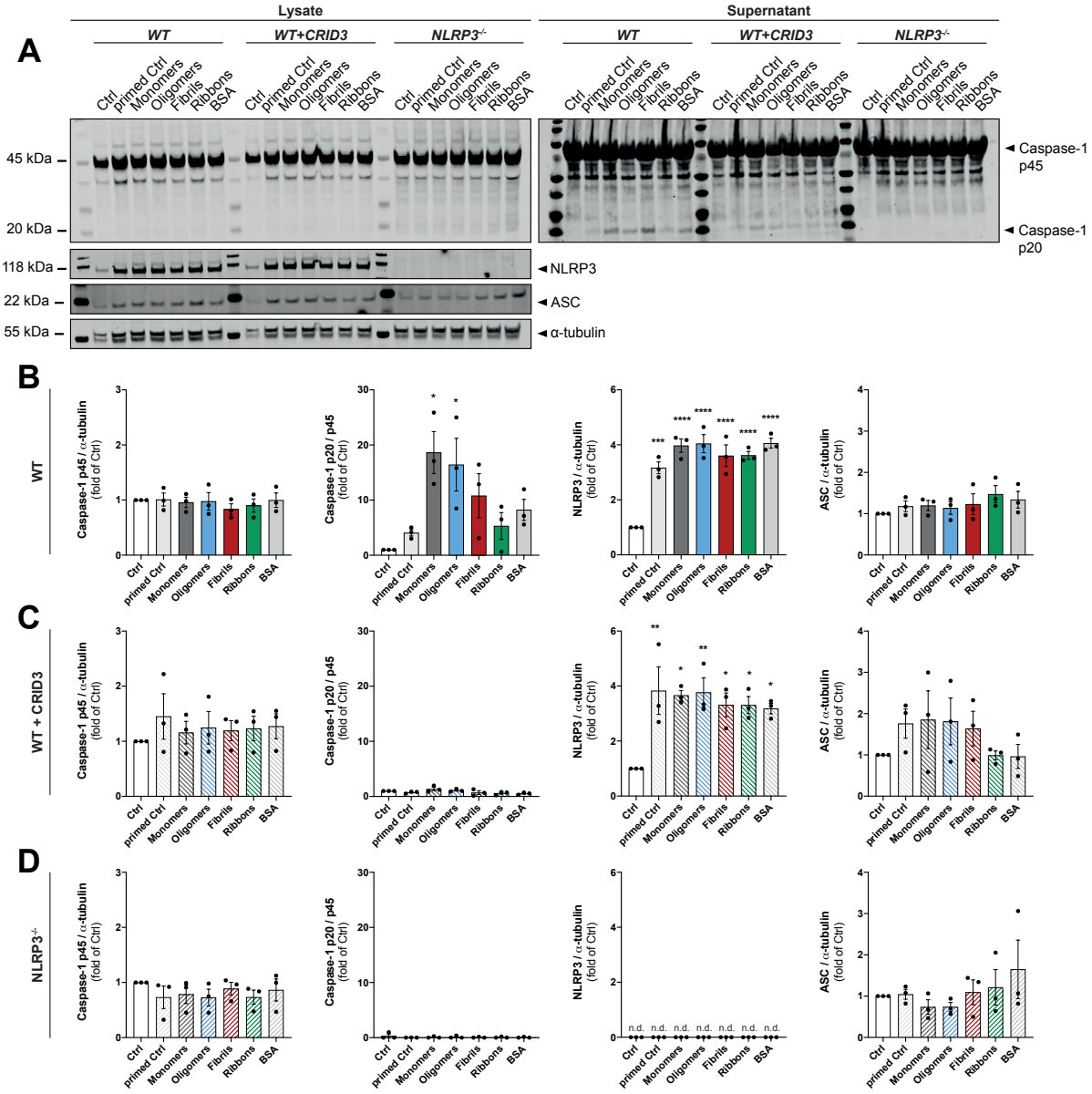

Figure S4
(A) Immunoblot of cell lysates (left) and supernatants (right) of primary microglia derived from WT or NLRP3$^{-/-}$ mice exposed to 2 μM α-syn and 200 nM CRID3 for 24 hrs. Blots were stained for caspase-1, NLRP3, ASC and α-tubulin. Quantification of Caspase-1 p45, cleaved Caspase-1 p20, NLRP3, and ASC in WT **(B)**, WT+CRID3 **(C)**, and NLRP3-/- **(D)**. n=3 independent experiments. All graphs are presented as mean ± SEM and were analysed by one-way ANOVA followed by Tukey's multiple comparison post hoc test. Levels of significance are: ****p < 0.0001, ***p < 0.001, **p < 0.01, *p < 0.05.

831

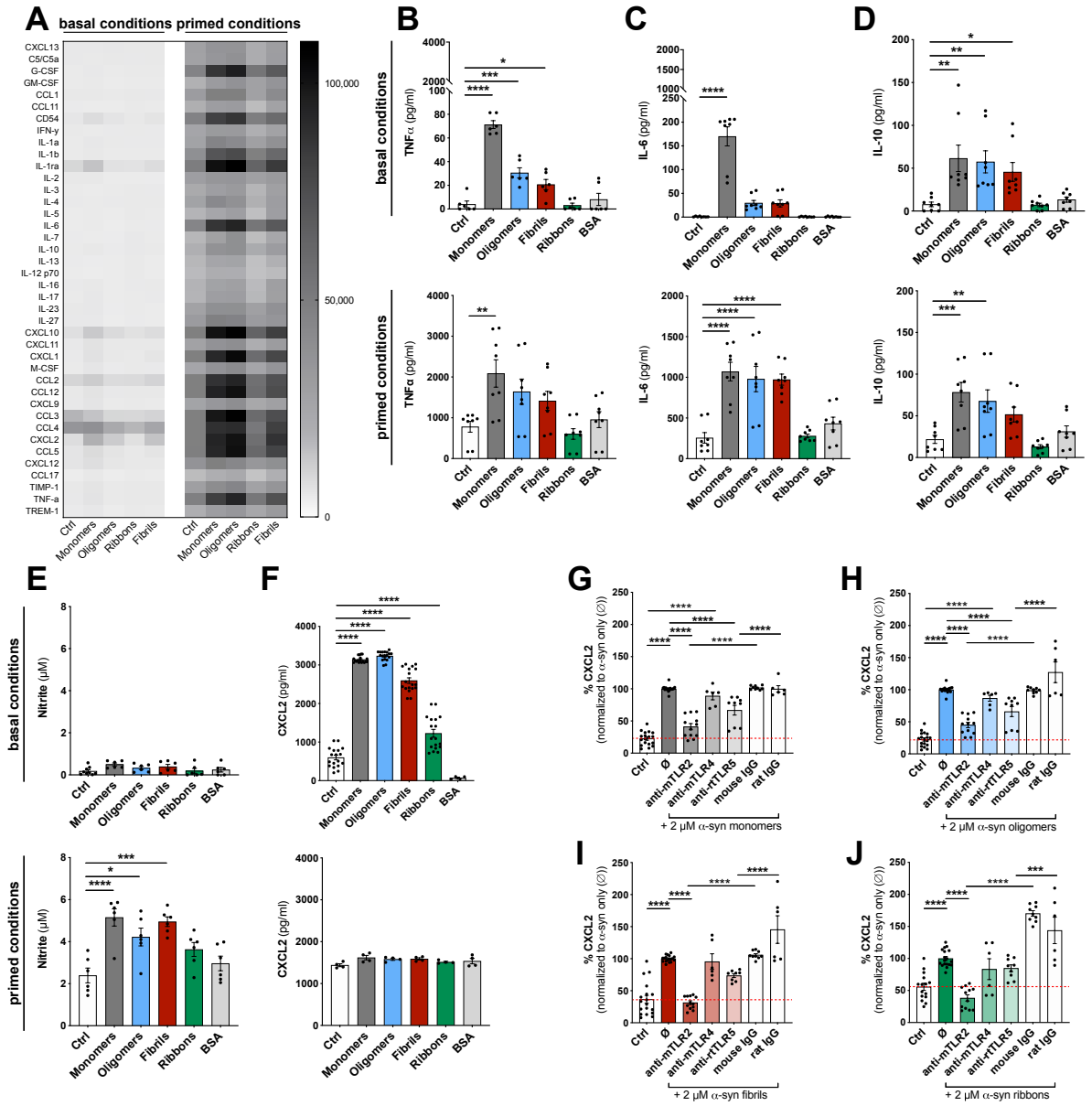

Figure S5

(A) Proteome profiling array on supernatants of primary microglia treated with 2 μM distinct α-syn forms without or with pre-exposure to LPS for 3 hrs. Quantification of TNFα **(B)**, IL-6 **(C)**, IL-10 **(D)**, Nitrite **(E)**, and CXCL2 **(F)** in supernatants of primary microglia treated with 2 μM distinct α-syn forms without (upper panel) or with (lower panel) pre-exposure to LPS for 3 hrs. (n=3-4 independent experiments with single, duplicate or triplicate measurements). CXCL2 levels in conditioned medium of unprimed primary microglia treated for 24 hrs with TLR2-, TLR4, and TLR5-neutralizing antibodies or the respective isotype controls in parallel to stimulation with α-syn monomers **(G)**, oligomers **(H)**, fibrils **(I)** and ribbons **(J)**. (n=4-6 independent experiments with duplicate or triplicate measurements). All graphs are presented as mean ± SEM and were analysed by one-way ANOVA followed by Tukey's multiple comparison post hoc test. Levels of significance are: ****p < 0.0001, ***p < 0.001, **p < 0.01, *p < 0.05.

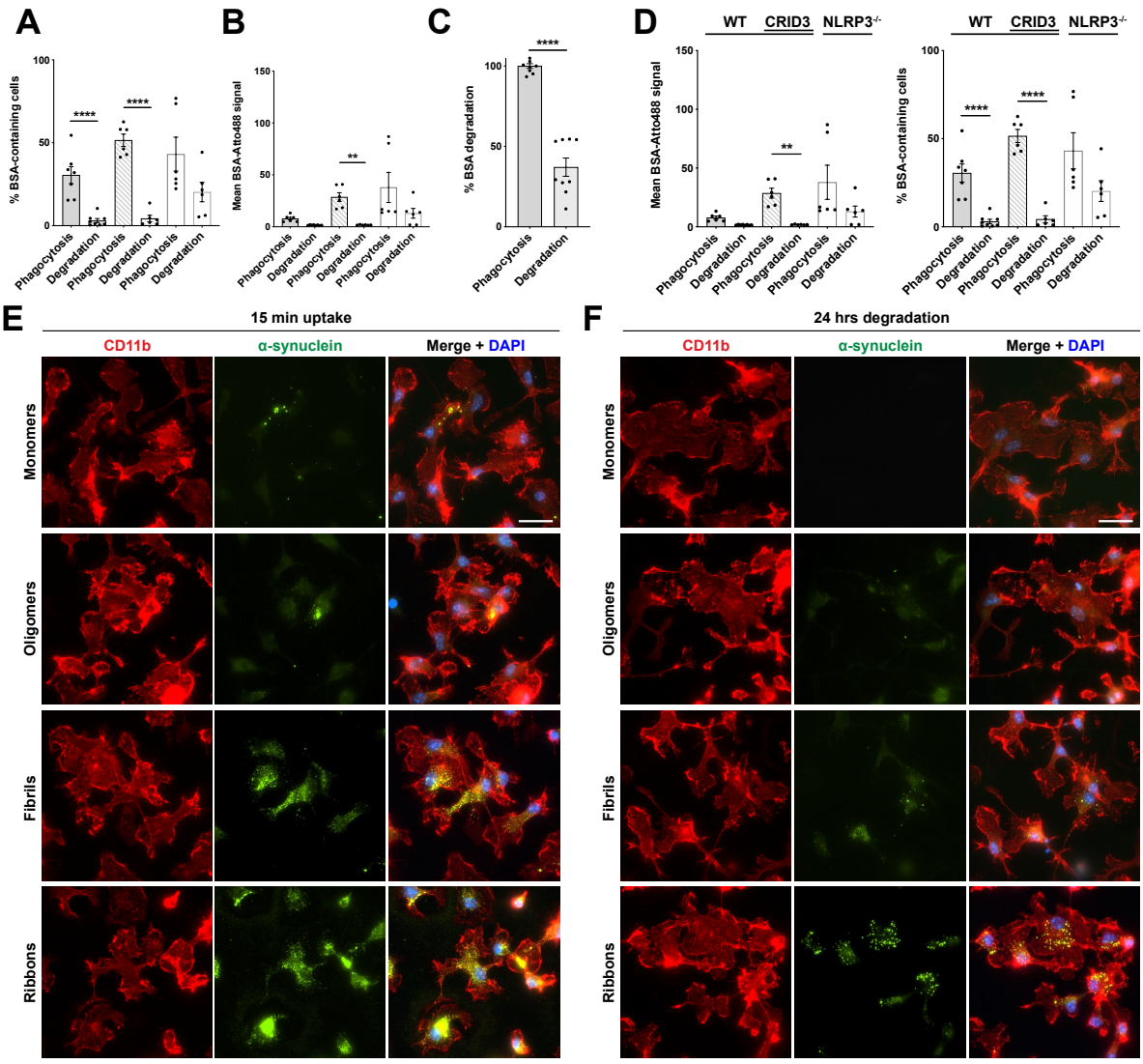

Figure S6
Quantification of the percent of phagocytic cells **(A)**, the phagocytic index **(B)**, and the percentage of degradation **(C)** of primary microglia exposed to BSA as protein control. (n=5-6 independent experiments). For comparison see also Fig. 4 and 5. **(D)** Quantification and comparison of phagocytosis and degradation of BSA by WT microglia (filled bars), WT microglia treated with the NLRP3 inflammasome inhibitor CRID3 (striped bars), or NLRP3-deficient microglia (empty bars). Representative immunostainings for CD11b-positive microglia (red) and distinct forms of α-syn-Atto488 (green) after 15 minutes of phagocytosis **(E)** or 24 hours of degradation **(F)**. All graphs are presented as mean ± SEM and were analysed by one-way ANOVA followed by Tukey's multiple comparison post hoc test. Levels of significance are: ****p < 0.0001, ***p < 0.001, **p < 0.01, *p < 0.05. Scale bar: 20 µm.

833